Published for SISSA by Springer

Received: *May 3, 2018*
Accepted: *September 24, 2018*
Published: *October 29, 2018*

Measurement of D^0, D^+, D^{*+} and D_s^+ production in Pb–Pb collisions at $\sqrt{s_{NN}} = 5.02$ TeV

The ALICE collaboration

E-mail: ALICE-publications@cern.ch

Abstract: We report measurements of the production of prompt D^0, D^+, D^{*+} and D_s^+ mesons in Pb–Pb collisions at the centre-of-mass energy per nucleon-nucleon pair $\sqrt{s_{NN}} = 5.02$ TeV, in the centrality classes 0–10%, 30–50% and 60–80%. The D-meson production yields are measured at mid-rapidity ($|y| < 0.5$) as a function of transverse momentum (p_T). The p_T intervals covered in central collisions are: $1 < p_T < 50$ GeV/c for D^0, $2 < p_T < 50$ GeV/c for D^+, $3 < p_T < 50$ GeV/c for D^{*+}, and $4 < p_T < 16$ GeV/c for D_s^+ mesons. The nuclear modification factors (R_{AA}) for non-strange D mesons (D^0, D^+, D^{*+}) show minimum values of about 0.2 for $p_T = 6$–10 GeV/c in the most central collisions and are compatible within uncertainties with those measured at $\sqrt{s_{NN}} = 2.76$ TeV. For D_s^+ mesons, the values of R_{AA} are larger than those of non-strange D mesons, but compatible within uncertainties. In central collisions the average R_{AA} of non-strange D mesons is compatible with that of charged particles for $p_T > 8$ GeV/c, while it is larger at lower p_T. The nuclear modification factors for strange and non-strange D mesons are also compared to theoretical models with different implementations of in-medium energy loss.

Keywords: Heavy Ion Experiments

ArXiv ePrint: 1804.09083

Open Access, Copyright CERN,
for the benefit of the ALICE Collaboration.
Article funded by SCOAP[3].

https://doi.org/10.1007/JHEP10(2018)174

JHEP10(2018)174

Contents

JHEP10(2018)174

1 Introduction

Ultra-relativistic collisions of heavy nuclei produce a state of strongly-interacting matter characterised by high energy density and temperature. According to Quantum Chromodynamics (QCD) on the lattice, in these extreme conditions matter undergoes a phase transition to a Quark-Gluon Plasma (QGP) state in which quarks and gluons are deconfined and chiral symmetry is partially restored [1–4].

Heavy quarks (such as charm and beauty) are predominantly produced in the early stage of the collision in hard scattering processes between partons of the incoming nuclei. Because of their large masses, their production time (~ 0.1 and $0.02\,\mathrm{fm}/c$ for charm and beauty, respectively [5]) is shorter than the formation time of the QGP, which is about 0.3–1.5 fm/c at Large Hadron Collider (LHC) energies [6]. In contrast, the thermal production and annihilation rates are negligible [7]. Heavy quarks therefore experience the full evolution of the hot and dense QCD medium.

During their propagation through the medium, heavy quarks are exposed to interactions with the medium constituents and lose part of their energy via inelastic (gluon radiation) [8, 9] or elastic scatterings (collisional processes) [10–12]. The colour-charge dependence of the strong interaction and parton-mass-dependent effects are predicted to influence the amount of energy loss (see [5, 13] for recent reviews). Low-momentum heavy quarks can participate in the collective expansion of the system as a consequence of multiple interactions with the medium [14, 15]. It was also suggested that low-momentum heavy quarks could hadronise not only via fragmentation in the vacuum, but also via the mechanism of recombination with other quarks in the medium [15, 16]. In this scenario,

the large abundance of strange quarks in nucleus-nucleus collisions with respect to proton-proton collisions is expected to lead to an increased production of $\mathrm{D_s^+}$ mesons relative to non-strange D mesons [17].

The effects of energy loss and the dynamics of heavy-quark hadronisation can be studied using the nuclear modification factor R_{AA}, which compares the transverse-momentum (p_{T}) differential production yields in nucleus-nucleus collisions ($\mathrm{d}N_{\mathrm{AA}}/\mathrm{d}p_{\mathrm{T}}$) with the cross section in proton-proton collisions ($\mathrm{d}\sigma_{\mathrm{pp}}/\mathrm{d}p_{\mathrm{T}}$) scaled by the average nuclear overlap function $\langle T_{\mathrm{AA}} \rangle$:

$$R_{\mathrm{AA}}(p_{\mathrm{T}}) = \frac{1}{\langle T_{\mathrm{AA}} \rangle} \cdot \frac{\mathrm{d}N_{\mathrm{AA}}/\mathrm{d}p_{\mathrm{T}}}{\mathrm{d}\sigma_{\mathrm{pp}}/\mathrm{d}p_{\mathrm{T}}} \,. \tag{1.1}$$

The average nuclear overlap function $\langle T_{\mathrm{AA}} \rangle$ is defined as the average number of nucleon-nucleon collisions $\langle N_{\mathrm{coll}} \rangle$, which can be estimated via Glauber model calculations [18–21], divided by the inelastic nucleon-nucleon cross section.

Measurements of prompt D-meson production by the ALICE collaboration in Pb–Pb collisions at $\sqrt{s_{\mathrm{NN}}} = 2.76\,\mathrm{TeV}$ [22–25] showed a strong suppression of the D-meson yields by a factor of 5–6 for $8 < p_{\mathrm{T}} < 12\,\mathrm{GeV}/c$ in the 10% most central collisions. Recent results from the CMS collaboration on $\mathrm{D^0}$ production in the p_{T} range 2–100 GeV/c show a similar suppression for $6 < p_{\mathrm{T}} < 10\,\mathrm{GeV}/c$ in the 10% most central Pb–Pb collisions at $\sqrt{s_{\mathrm{NN}}} = 5.02\,\mathrm{TeV}$, decreasing with increasing p_{T} [26]. In contrast, the D-meson nuclear modification factor in p–Pb collisions at $\sqrt{s_{\mathrm{NN}}} = 5.02\,\mathrm{TeV}$, where an extended QGP phase is not expected to be formed, was found to be consistent with unity within uncertainties for $0 < p_{\mathrm{T}} < 24\,\mathrm{GeV}/c$ [27]. These results indicate that the strong suppression is due to substantial final-state interactions of charm quarks with the QGP formed in Pb–Pb collisions.

In this article, we present the measurement of p_{T}-differential yields and the nuclear modification factor for prompt $\mathrm{D^0}$, $\mathrm{D^+}$, $\mathrm{D^{*+}}$ and $\mathrm{D_s^+}$ mesons (including their antiparticles), in Pb–Pb collisions at $\sqrt{s_{\mathrm{NN}}} = 5.02\,\mathrm{TeV}$ collected with the ALICE detector during the LHC Run 2 in 2015. Prompt D mesons are defined as those produced by the hadronisation of charm quarks or from the decay of excited open charm and charmonium states, hence excluding the decays of beauty hadrons. The experimental apparatus is briefly presented in section 2, together with the data sample used for the analysis. The reconstruction of D-meson hadronic decays and all corrections applied to the raw yields are presented in section 3. The procedure used to obtain the proton-proton reference cross section at $\sqrt{s} = 5.02\,\mathrm{TeV}$ and the estimation of the systematic uncertainties are described in section 4 and section 5, respectively. The results for the central (0–10%), semi-central (30–50%) and peripheral (60–80%) collisions are presented in section 6. A comparison with charged-pion and charged-particle R_{AA} is reported in the same section, along with detailed comparisons with model calculations, including a simultaneous comparison of the R_{AA} and elliptic flow v_2. Conclusions are drawn in section 7.

2 Experimental apparatus and data sample

A description of the ALICE experimental apparatus and its performance in pp, p–Pb and Pb–Pb collisions can be found in [28, 29]. The main detectors used in the present analysis

JHEP10(2018)174

Centrality class	$\langle T_{\rm AA} \rangle$ (mb^{-1})	$N_{\rm events}$
0–10%	23.07 ± 0.44	10.4×10^6
30–50%	3.90 ± 0.11	20.8×10^6
60–80%	0.417 ± 0.014	20.8×10^6

Table 1. Average nuclear overlap function and number of events for the three centrality classes used in the analysis.

are the V0 detector, the Inner Tracking System (ITS) [30], the Time Projection Chamber (TPC) [31] and the Time Of Flight (TOF) detector [32], located inside a large solenoidal magnet providing a uniform magnetic field of 0.5 T parallel to the LHC beam direction (z axis in the ALICE reference system), and the Zero Degree Calorimeters (ZDC) [33], located at $z = \pm 112.5$ m from the nominal interaction point. The analysed sample consists of Pb–Pb collision data recorded with a minimum-bias interaction trigger that required coincident signals in both scintillator arrays of the V0 detector [34]. The V0 detector consists of two scintillator arrays, which cover the full azimuth in the pseudorapidity intervals $-3.7 < \eta < -1.7$ and $2.8 < \eta < 5.1$. Events produced by the interaction of the beams with residual gas in the vacuum pipe were rejected offline using the V0 and the ZDC timing information. Only events with a reconstructed interaction point (primary vertex) within ± 10 cm from the centre of the ITS detector along the beam line were used in the analysis. For the data sample considered in this paper, the probability of in-bunch collision pileup (i.e. collisions with two or more simultaneous interactions per bunch crossing) was negligible, while the request of at least a hit in one of the two innermost layers of the ITS rejected tracks produced in out-of-bunch pileup collisions.

Collisions were divided into centrality classes, determined from the sum of the V0 signal amplitudes and defined in terms of percentiles of the hadronic Pb–Pb cross section. In order to relate the centrality classes to the collision geometry, the distribution of the V0 summed amplitudes was fitted with a function based on the Glauber model [18–21] combined with a two-component model for particle production [35], which decomposes particle production in nucleus-nucleus collisions into the contributions due to soft and hard interactions. The centrality classes used in the present analysis, together with the corresponding average nuclear overlap function $\langle T_{\rm AA} \rangle$ [36] and the number of events ($N_{\rm events}$) in each class, are summarised in table 1. The corresponding integrated luminosity is about $L_{\rm int} \approx 13\,\mu{\rm b}^{-1}$ [37].

3 Data analysis

The D mesons and their charge conjugates were reconstructed in the decay channels $\rm D^0 \to K^-\pi^+$ (with branching ratio, BR, of $(3.93 \pm 0.04)\%$), $\rm D^+ \to K^-\pi^+\pi^+$ (BR of $(9.46 \pm 0.24)\%$), $\rm D^{*+} \to D^0\pi^+$ (BR of $(67.7 \pm 0.5)\%$) and $\rm D_s^+ \to \phi\pi^+ \to K^+K^-\pi^+$ (BR of $(2.27 \pm 0.08)\%$) [38]. $\rm D^0$, $\rm D^+$ and $\rm D_s^+$ candidates were defined using pairs and triplets of tracks with proper charge-sign combination having $|\eta| < 0.8$, $p_{\rm T} > 0.4$ GeV/c, a minimum number of 70 (out of 159) associated space points in the TPC and at least two hits

JHEP10(2018)174

(out of six) in the ITS, with at least one in the two innermost layers. D^{*+} candidates were formed by combining D^0 candidates with tracks having $|\eta| < 0.8$, $p_{\mathrm{T}} > 0.1\,\mathrm{GeV}/c$ and at least three associated hits in the ITS. For $\mathrm{D}_{\mathrm{s}}^+$ candidate selection, one of the two pairs of opposite-sign tracks was required to have an invariant mass compatible with the ϕ mass ($m_\phi = 1019.461 \pm 0.019\,\mathrm{MeV}/c^2$ [38]). In particular, the difference between the reconstructed $\mathrm{K}^+\mathrm{K}^-$ invariant mass and ϕ mass was required to be less than 5–10 MeV/c^2 depending on the $\mathrm{D}_{\mathrm{s}}^+$ p_{T} interval. This selection preserves 70–85% of the $\mathrm{D}_{\mathrm{s}}^+$ signal.

The selection of tracks with $|\eta| < 0.8$ limits the D-meson acceptance in rapidity, which, depending on p_{T}, varies from $|y| < 0.6$ for $p_{\mathrm{T}} = 1\,\mathrm{GeV}/c$ to $|y| < 0.8$ for $p_{\mathrm{T}} > 5\,\mathrm{GeV}/c$. A p_{T}-dependent fiducial acceptance cut, $|y_{\mathrm{D}}| < y_{\mathrm{fid}}(p_{\mathrm{T}})$, was therefore applied to the D-meson rapidity. The value of $y_{\mathrm{fid}}(p_{\mathrm{T}})$ increases from 0.6 to 0.8 in the range $1 < p_{\mathrm{T}} < 5\,\mathrm{GeV}/c$, and the variation can be described according to a second-order polynomial function. For $p_{\mathrm{T}} > 5\,\mathrm{GeV}/c$ one has $y_{\mathrm{fid}} = 0.8$.

The selection strategy is similar to the one used in previous analyses [25, 39] and is mainly based on the separation between primary and secondary vertex, the displacement of the tracks from the primary vertex and the pointing of the reconstructed D-meson momentum to the primary vertex. In comparison to previous analyses, additional selection criteria were exploited. In particular, the normalised difference between the measured and expected transverse-plane impact parameters of each of the decay particles (already introduced in [40]) and the transverse-plane impact parameter to the primary vertex (d_0^{xy}) of the D-meson candidates were used. Besides the rejection of the combinatorial background, a selection based on the latter two variables has the advantage to suppress significantly the fraction of D mesons coming from beauty-hadron decays (feed-down) and hence reduce the associated systematic uncertainty. The cut values on the selection variables were optimised in each centrality class independently, in order to obtain a large statistical significance of the D-meson signals, while keeping the selection efficiency of promptly produced D mesons as large as possible. Further background reduction was obtained by applying particle identification for charged pions and kaons with the TPC and TOF detectors. A $\pm 3\,\sigma$ window around the expected mean values of specific ionisation energy loss $\mathrm{d}E/\mathrm{d}x$ in the TPC gas and time-of-flight from the interaction point to the TOF detector was used for the identification, where σ is the resolution on these two quantities. In central collisions, a $2\,\sigma$ selection was used for D^{*+} and D^+ (for $p_{\mathrm{T}} < 3\,\mathrm{GeV}/c$) candidates. For $\mathrm{D}_{\mathrm{s}}^+$ candidates, tracks without a TOF signal (mostly at low momentum) were identified using only the TPC information and requiring a $2\,\sigma$ compatibility with the expected $\mathrm{d}E/\mathrm{d}x$. The stricter PID selection strategy was needed due to the large background of track triplets and, in case of $\mathrm{D}_{\mathrm{s}}^+$, because of its short lifetime, which limits the effectiveness of the geometrical selections on the displaced decay-vertex topology.

The D^0, D^+ and $\mathrm{D}_{\mathrm{s}}^+$ raw yields were obtained from binned maximum-likelihood fits to the candidate invariant-mass (M) distributions, while for the D^{*+} the mass difference $\Delta M = M(\mathrm{K}\pi\pi) - M(\mathrm{K}\pi)$ distributions were used. Examples for these distributions are shown in figure 1 for the centrality class 0–10%. The D^0, D^+ and $\mathrm{D}_{\mathrm{s}}^+$ candidate invariant-mass distributions were fitted with a function composed of a Gaussian term for the signal and an exponential function to describe the background shape, with the exception of the

JHEP10(2018)174

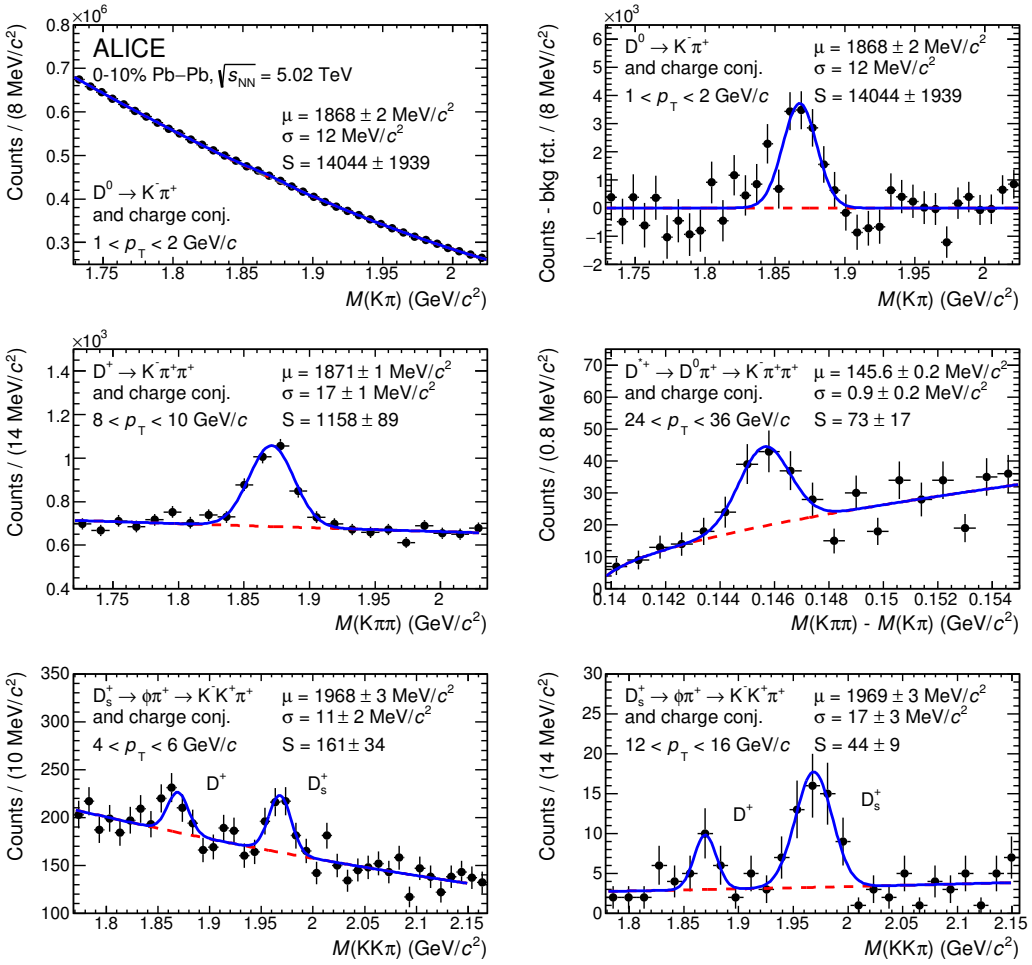

Figure 1. Invariant-mass distributions for the four D-meson species in selected p_{T} intervals for the centrality class 0–10%. Fitted values for the meson mass μ, width σ and raw yield S are also given. Top row: D^0 mesons with $1 < p_{\mathrm{T}} < 2\,\mathrm{GeV}/c$, before (left) and after (right) subtraction of the background fit function. For this p_{T} interval, the width of the Gaussian used to describe the signal is fixed to the value obtained in the simulations. Middle row: D^+ mesons with $8 < p_{\mathrm{T}} < 10\,\mathrm{GeV}/c$ and D^{*+} mesons (difference of $M(\mathrm{K}\pi\pi)$ and $M(\mathrm{K}\pi)$) with $24 < p_{\mathrm{T}} < 36\,\mathrm{GeV}/c$. Bottom row: $\mathrm{D}_{\mathrm{s}}^+$ mesons with $4 < p_{\mathrm{T}} < 6\,\mathrm{GeV}/c$ and $12 < p_{\mathrm{T}} < 16\,\mathrm{GeV}/c$; the $\mathrm{D}^+ \to \mathrm{K}^+\mathrm{K}^-\pi^+$ signal is visible on the left of the $\mathrm{D}_{\mathrm{s}}^+$ signal.

D^0 p_{T} intervals 1–2 GeV/c and 2–3 GeV/c, where the background was found to be better described by a second-order polynomial function (a fourth-order polynomial was used in 1–2 GeV/c for the 0–10% centrality class). The ΔM distribution of D^{*+} candidates was fitted with a Gaussian function for the signal and a threshold function multiplied by an exponential for the background ($a\sqrt{\Delta M - m_\pi}\cdot \mathrm{e}^{b(\Delta M - m_\pi)}$, where m_π is the pion mass and a and b are free parameters). The contribution of signal candidates that are present in the invariant-mass distribution of the D^0 meson with the wrong decay-particle mass assignment (reflection), was parametrised by fitting the simulated reflection invariant-mass distributions with a double Gaussian function, and it was included in the total D^0 fit function. The ratio between the reflected signal and the yields of the D^0 was taken from simulations

JHEP10(2018)174

(typically 2–5% of the raw yield, depending on $p_{\rm T}$) [39]. The Monte Carlo simulation used for this study is the same one used to determine the reconstruction efficiency, as described in the following dedicated paragraph. In addition, given the critical signal extraction induced by the small signal-to-background ratio of the $\rm D^0$ meson in $1 < p_{\rm T} < 2\,\mathrm{GeV}/c$, the width of the Gaussian used to describe the signal was fixed to the value obtained in the simulations. The Gaussian widths obtained from the simulations were found to be consistent with those extracted from the data in the full $p_{\rm T}$ range, for all measured centrality classes, with deviations of at most 10–15%. In the fit to the $\rm D_s^+$-candidate invariant-mass distribution, an additional Gaussian was used to describe the $\rm D^+ \to K^+K^-\pi^+$ signal on the left of the $\rm D_s^+$ signal. The statistical significance $\mathrm{S}/\sqrt{\mathrm{S}+\mathrm{B}}$ of the observed signals, estimated within 3 standard deviations, varies from 5 to 33 depending on the D-meson species, the $p_{\rm T}$ interval, and the centrality class.

The D-meson raw yields were corrected in order to obtain the $p_{\rm T}$-differential yields of prompt D mesons

$$\left.\frac{\mathrm{d}N^{\rm D}}{\mathrm{d}p_{\rm T}}\right|_{|y|<0.5} = \frac{f_{\rm prompt}(p_{\rm T}) \cdot \frac{1}{2} N_{\rm raw}^{\rm D+\overline{D}}(p_{\rm T})\Big|_{|y|<y_{\rm fid}(p_{\rm T})}}{\Delta p_{\rm T} \cdot \alpha_y(p_{\rm T}) \cdot (\mathrm{Acc}\times\epsilon)_{\rm prompt}(p_{\rm T}) \cdot \mathrm{BR} \cdot N_{\rm events}}\,. \tag{3.1}$$

The raw yields $N_{\rm raw}^{\rm D+\overline{D}}$ were divided by a factor of two to obtain the charge-averaged (particle and antiparticle) yields. To correct for the contribution of feed-down from beauty-hadron decays, the raw yields were multiplied by the fraction of promptly produced D mesons, $f_{\rm prompt}$ (see eq. (3.2)). Furthermore, they were divided by the product of prompt D-meson acceptance and efficiency $(\mathrm{Acc}\times\epsilon)_{\rm prompt}$, by the branching ratio BR of the decay channel, by the transverse momentum interval width $\Delta p_{\rm T}$ and by the number of events $N_{\rm events}$. The $(\mathrm{Acc}\times\epsilon)_{\rm prompt}$ correction includes the tracking efficiency, the acceptance of pions and kaons, and the kinematical and topological selection efficiency of D mesons. The factor $\alpha_y(p_{\rm T}) = y_{\rm fid}(p_{\rm T})/0.5$ normalises the corrected yields measured in $|y| < y_{\rm fid}(p_{\rm T})$ to one unit of rapidity $|y| < 0.5$, assuming a flat rapidity distribution for D mesons in $|y| < y_{\rm fid}(p_{\rm T})$. This assumption was validated to the 1% level with simulations for pp collisions [41, 42] and it is justified also for Pb–Pb collisions. For example, measurements of the prompt and non-prompt J/ψ $R_{\rm AA}$ in Pb–Pb collisions at $\sqrt{s_{\rm NN}} = 2.76\,\mathrm{TeV}$ do not exhibit a significant rapidity dependence [43].

The correction for acceptance and efficiency $(\mathrm{Acc}\times\epsilon)_{\rm prompt}$ was determined using Monte Carlo simulations with a detailed description of the detector and its response, based on the GEANT3 transport package [44]. The underlying Pb–Pb events at $\sqrt{s_{\rm NN}} = 5.02\,\mathrm{TeV}$ were simulated using the HIJING v1.383 generator [45] and D-meson signals were added using the PYTHIA v6.421 generator [46] with Perugia-2011 tune. Each simulated PYTHIA pp event contained a $\rm c\overline{c}$ or $\rm b\overline{b}$ pair, and D mesons were forced to decay into the hadronic channels of interest for the analysis. In the most central event class, the $p_{\rm T}$ distribution of D mesons in the MC simulation for $p_{\rm T} > 2\,\mathrm{GeV}/c$ was weighted in order to match the shape measured in data for $\rm D^0$ mesons in finer $p_{\rm T}$ intervals with respect to those used in the analysis. In the centrality classes and $p_{\rm T}$ ranges where an analysis in finer $p_{\rm T}$ intervals was not possible, the simulated D-meson $p_{\rm T}$ distribution was weighted to match the shape

JHEP10(2018)174

given by model calculations. In particular, fixed-order plus next-to-leading-log perturbative QCD calculations (FONLL) [47, 48] multiplied by the $R_{\rm AA}(p_{\rm T})$ of D mesons computed using the BAMPS model (which implements both elastic and radiative processes) for the 30–50% centrality class [49–51] were used for the corresponding centrality class. For the $p_{\rm T}$ intervals 1–2 GeV/c and 16–50 GeV/c in the 0–10% centrality class and for the 60–80% centrality class, where the $R_{\rm AA}$ is nearly flat in the measured $p_{\rm T}$ interval, only the FONLL calculations were used.

Figure 2 shows the acceptance-times-efficiency (Acc $\times\,\varepsilon$) for prompt and feed-down D mesons with rapidity $|y| < y_{\rm fid}(p_{\rm T})$ in the centrality class 0–10%, after the aforementioned $p_{\rm T}$-distribution weighting procedure. The difference between the (Acc$\times\varepsilon$) factor for prompt and feed-down D mesons arises from the geometrical selections applied, given the different decay topology of D mesons coming from B decays. In particular, the feed-down D mesons are on average more displaced from the primary vertex due to the large B-meson lifetime ($c\tau \approx 500\,\mu$m [38]) and therefore are more efficiently selected by the majority of the analysis cuts (e.g. for $\rm D^0$ and $\rm D^{*+}$ in most of the $p_{\rm T}$ intervals). On the contrary, the selections on the difference between measured and expected decay-track impact parameters and on the D-meson impact parameter reject more feed-down D mesons, thus reducing the feed-down efficiencies as compared to the previous analyses (e.g. for $\rm D^+$ and $\rm D_s^+$). The (Acc $\times\,\varepsilon$) is higher for more peripheral collisions, by up to a factor larger than two at low $p_{\rm T}$, since less stringent selections can be applied because of the lower combinatorial background.

The $f_{\rm prompt}$ factor was obtained, following the procedure introduced in [22], by subtracting the contribution of D mesons from beauty-hadron decays from the measured raw yield in each $p_{\rm T}$ interval. It was estimated using perturbative QCD calculations, efficiencies from MC simulations, and an hypothesis on the $R_{\rm AA}$ of feed-down D mesons. The expression for $f_{\rm prompt}$ reads:

$$
\begin{aligned}
f_{\rm prompt} &= 1 - \frac{N_{\rm raw}^{\rm D+\overline{D}\,feed\text{-}down}}{N_{\rm raw}^{\rm D+\overline{D}}} \\
&= 1 - R_{\rm AA}^{\rm feed\text{-}down} \cdot \langle T_{\rm AA} \rangle \cdot \left(\frac{{\rm d}\sigma}{{\rm d}p_{\rm T}} \right)^{\rm FONLL,\,EvtGen}_{\rm feed\text{-}down,\,|y|<0.5} \cdot \frac{\Delta p_{\rm T} \cdot \alpha_y \cdot ({\rm Acc} \times \epsilon)_{\rm feed\text{-}down} \cdot {\rm BR} \cdot N_{\rm events}}{\frac{1}{2} N_{\rm raw}^{\rm D+\overline{D}}} \,.
\end{aligned}
\tag{3.2}
$$

In this expression, $N_{\rm raw}^{\rm D+\overline{D}}$ is the measured raw yield and $N_{\rm raw}^{\rm D+\overline{D}\,feed\text{-}down}$ is the estimated raw yield of D mesons from beauty-hadron decays. In detail, the beauty-hadron production cross section in pp collisions at $\sqrt{s} = 5.02$ TeV, estimated with FONLL calculations [52], was folded with the beauty-hadron$\rightarrow$ D + X decay kinematics using the EvtGen package [53] and multiplied by $\langle T_{\rm AA} \rangle$ of the corresponding centrality class, by the (Acc $\times\,\varepsilon$) for feed-down D mesons, and by the other factors introduced in eq. (3.1). In addition, the nuclear modification factor of D mesons from beauty-hadron decays was accounted for. The comparison of the $R_{\rm AA}$ of prompt D mesons ($R_{\rm AA}^{\rm prompt}$) at $\sqrt{s_{\rm NN}} = 2.76$ TeV [24] with that of J/ψ from B-meson decays [43] at the same energy measured by the CMS collaboration indicates that prompt charmed hadrons are more suppressed than non-prompt charmed hadrons. The $R_{\rm AA}$ values differ by a factor of about two in central collisions at a transverse momentum of about 10 GeV/c [24] and this difference is described by model

JHEP10(2018)174

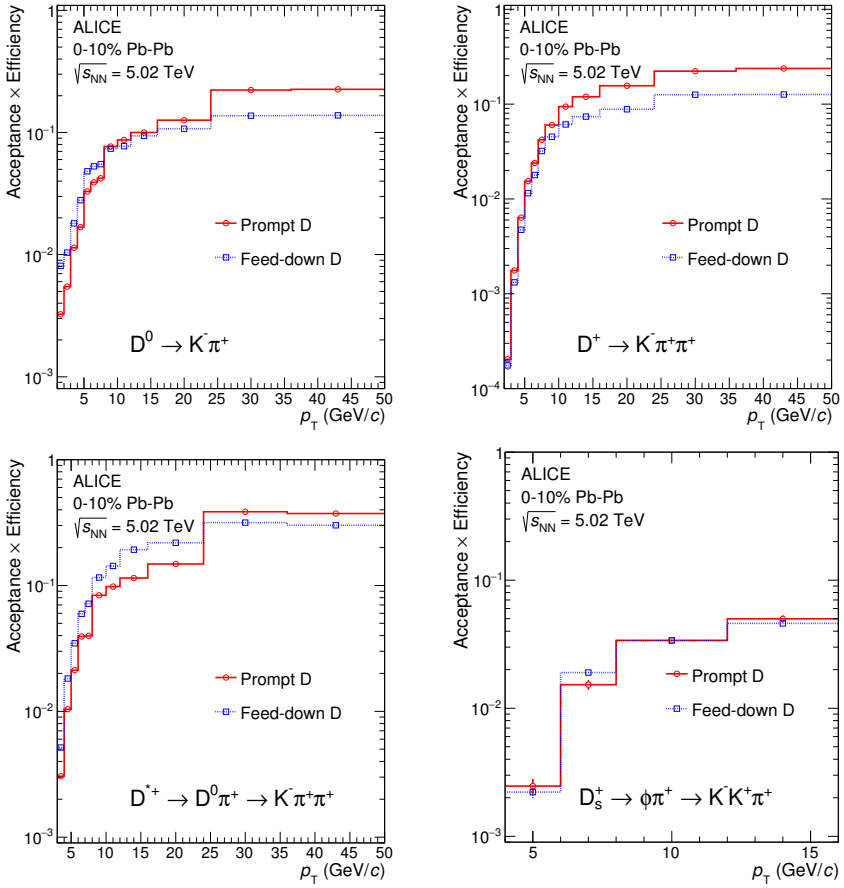

Figure 2. Product of acceptance and efficiency as a function of p_{T} for prompt (red circles) and feed-down (blue squares) D mesons in Pb–Pb collisions for the 0–10% centrality class obtained from MC simulations.

calculations with parton-mass-dependent energy loss. Therefore, for the centrality classes 0–10% and 30–50%, the value $R_{\mathrm{AA}}^{\text{feed-down}} = 2 \cdot R_{\mathrm{AA}}^{\text{prompt}}$ was used to compute the correction for non-strange D mesons with $3 < p_{\mathrm{T}} < 24\,\mathrm{GeV}/c$. This hypothesis was varied in the range $1 < R_{\mathrm{AA}}^{\text{feed-down}}/R_{\mathrm{AA}}^{\text{prompt}} < 3$ considering the data uncertainties and model variations to estimate a systematic uncertainty. For $1 < p_{\mathrm{T}} < 3\,\mathrm{GeV}/c$ and $24 < p_{\mathrm{T}} < 50\,\mathrm{GeV}/c$, where model calculations predict a reduced difference between the R_{AA} values of prompt and non-prompt charm hadrons [54, 55], the hypothesis $R_{\mathrm{AA}}^{\text{feed-down}} = 1.5 \cdot R_{\mathrm{AA}}^{\text{prompt}}$ was used, with a variation in $1 < R_{\mathrm{AA}}^{\text{feed-down}}/R_{\mathrm{AA}}^{\text{prompt}} < 2$ for the systematic uncertainty. In the case of strange D mesons, effects induced by the in-medium hadronisation and increased abundance of strange quarks could influence the ratio of the R_{AA} values of prompt and feed-down $\mathrm{D_s^+}$. Therefore, more conservative central values and variation ranges for the hypothesis were used for $\mathrm{D_s^+}$ mesons, namely $R_{\mathrm{AA}}^{\text{feed-down}} = R_{\mathrm{AA}}^{\text{prompt}}$ and $\frac{1}{3} < R_{\mathrm{AA}}^{\text{feed-down}}/R_{\mathrm{AA}}^{\text{prompt}} < 3$. For the peripheral class 60–80%, in which the medium effects are milder, also the difference between charm and beauty mesons is assumed to be reduced: the value $R_{\mathrm{AA}}^{\text{feed-down}} = 1.5 \cdot R_{\mathrm{AA}}^{\text{prompt}}$, varied in the range $1 < R_{\mathrm{AA}}^{\text{feed-down}}/R_{\mathrm{AA}}^{\text{prompt}} < 2$, was used for all D-meson species. The resulting f_{prompt} values, for the central hypotheses on $R_{\mathrm{AA}}^{\text{feed-down}}/R_{\mathrm{AA}}^{\text{prompt}}$, range from about

JHEP10(2018)174

0.80 to 0.95, depending on the D-meson species, centrality class and p_{T} interval. The systematic uncertainties obtained from the variation of the hypotheses are discussed in section 5.

4 Proton-proton reference for R_{AA}

The p_{T}-differential cross sections of prompt D mesons with $|y| < 0.5$ in pp collisions at $\sqrt{s} = 5.02\,\mathrm{TeV}$, used as reference for the nuclear modification factor, were obtained by scaling the measurements at $\sqrt{s} = 7\,\mathrm{TeV}$ [40] to $\sqrt{s} = 5.02\,\mathrm{TeV}$ with FONLL calculations [52]. These measurements reach up to $p_{\mathrm{T}} = 36\,\mathrm{GeV}/c$ for D^0, $24\,\mathrm{GeV}/c$ for D^+ and D^{*+}, and $12\,\mathrm{GeV}/c$ for $\mathrm{D}_{\mathrm{s}}^+$ mesons. The uncertainties on the p_{T}-dependent scaling factor from $\sqrt{s} = 7\,\mathrm{TeV}$ to $\sqrt{s} = 5.02\,\mathrm{TeV}$ were determined by varying the FONLL parameters (charm-quark mass, factorisation and renormalisation scales) as described in [56]. The uncertainties range from $^{+17}_{-4}\%$ for $1 < p_{\mathrm{T}} < 2\,\mathrm{GeV}/c$ to about $\pm 3\%$ for $p_{\mathrm{T}} > 10\,\mathrm{GeV}/c$.

At high D-meson p_{T} ($36 < p_{\mathrm{T}} < 50\,\mathrm{GeV}/c$ for D^0, $24 < p_{\mathrm{T}} < 50\,\mathrm{GeV}/c$ for D^+ and D^{*+}, and $12 < p_{\mathrm{T}} < 16\,\mathrm{GeV}/c$ for $\mathrm{D}_{\mathrm{s}}^+$), the FONLL calculation at $\sqrt{s} = 5.02\,\mathrm{TeV}$ [52] was used as a reference by scaling the values for each meson species to match the central value of the scaled data at lower p_{T}. This procedure is described in ref. [23]. As an example, the total systematic uncertainties on the pp reference for D^0 mesons with $36 < p_{\mathrm{T}} < 50\,\mathrm{GeV}/c$ is $^{+38}_{-28}\%$.

5 Systematic uncertainties

Systematic uncertainties on the D-meson yield in Pb–Pb collisions were estimated considering the following sources: (i) extraction of the raw yield from the invariant-mass distributions; (ii) track reconstruction efficiency; (iii) D-meson selection efficiency; (iv) PID efficiency; (v) generated D-meson p_{T} shape in the simulation; (vi) subtraction of the feed-down from beauty-hadron decays. In addition, the uncertainties on the branching ratios [38] were considered. A procedure similar to that described in [22–25] and outlined in what follows was used to estimate the uncertainties as a function of p_{T} and centrality. The systematic uncertainties on the raw yield extraction were evaluated for each D-meson species and in each p_{T} interval by varying the lower and upper limits of the fit range, and the background fit function. In addition, the same approach was used with a bin-counting method, in which the signal yield was obtained by integrating the invariant-mass distribution after subtracting the background estimated from a fit to the side-bands. It ranges between 2% and 15% depending on the D-meson species and p_{T} interval. In the case of D^0, an additional contribution due to signal reflections in the invariant-mass distribution was estimated by varying the ratio of the integral of the reflections over the integral of the signal and the shape of the templates used in the invariant-mass fits. For the D^0 meson in the interval $1 < p_{\mathrm{T}} < 2\,\mathrm{GeV}/c$, the signal line shape was varied by using Gaussian functions with the widths fixed to $\pm 15\%$ with respect to the value expected from Monte Carlo simulations, based on the deviations between the Gaussian width values observed in

JHEP10(2018)174

data and simulations. For the four D mesons, further checks on the stability of the results were performed by repeating the fits varying the invariant-mass bin width.

The systematic uncertainty on the track reconstruction efficiency was estimated by varying the track-quality selection criteria and by comparing the probability to match the TPC tracks to the ITS hits in data and simulation. The comparison of the matching efficiency in data and simulations was made after weighting the relative abundances of primary and secondary particles in the simulation to match those observed in data, which were estimated via fits to the inclusive track impact parameter distributions. The estimated uncertainty depends on the D-meson p_{T} and ranges from 3% to 8% for the two-body decay of D^0 mesons and from 6% to 12% for the three-body decays of D^+, D^{*+} and $\mathrm{D}_{\mathrm{s}}^+$ mesons.

To estimate the uncertainty on the PID selection efficiency, for the three non-strange D-meson species the analysis was repeated without PID selection. The resulting cross sections were found to be compatible with those obtained with the PID selection and therefore no systematic uncertainty was assigned. For the $\mathrm{D}_{\mathrm{s}}^+$ meson, the lower signal yield and the larger combinatorial background prevented a signal estimation without particle identification. In this case, a 3% uncertainty was estimated by repeating the analysis with a $3\,\sigma$ PID selection, similar to that used for non-strange D-mesons for which no systematic effects were observed. This value was also verified by comparing the pion and kaon PID selection efficiencies in the data and in the simulation and combining the observed differences using the $\mathrm{D}_{\mathrm{s}}^+$ decay kinematics (for this test, pure pion samples were selected using strange hadron decays, while kaon samples in the TPC were obtained using a tight PID selection in the TOF).

The uncertainty on the D-meson selection efficiency (see Cut efficiency in table 2) originates from imperfections in the description of the D-meson kinematic properties and of the detector resolutions and alignments in the simulation. It was estimated by comparing the corrected yields obtained by repeating the analysis with different sets of selection criteria resulting in a significant modification of the efficiencies, raw yield and background values. The assigned uncertainty for non-strange D mesons is 5% in most of the p_{T} intervals and it increases to 10–15% in the lowest p_{T} intervals, where the efficiencies are low and vary steeply with p_{T}, because of the tighter selections. A larger uncertainty of 10% in all p_{T} intervals was estimated for $\mathrm{D}_{\mathrm{s}}^+$ mesons, for which more stringent selection criteria were utilized in the analysis as compared to non-strange D mesons.

The systematic effect on the efficiency due to a possible difference between the real and simulated D-meson transverse momentum distributions was estimated by using alternative D-meson p_{T} distributions. In particular, the p_{T} distributions from FONLL calculations with and without hot-medium effects parametrised based on the R_{AA} in central collisions from the BAMPS [57], LBT [58] and TAMU [55] models were used in this study. The uncertainty, which also includes the effect of the p_{T} dependence of the nuclear modification factor, was estimated to be, for non-strange D mesons in central collisions, about 10% in the lowest p_{T} intervals and decreasing to zero for $p_{\mathrm{T}} > 5\,\mathrm{GeV}/c$. For $\mathrm{D}_{\mathrm{s}}^+$ mesons the uncertainty was estimated as 7% in 4–6 GeV/c, 2% in 6–8 GeV/c and 1% at higher p_{T}.

The systematic uncertainty on the subtraction of feed-down from beauty-hadron decays (i.e. the calculation of the f_{prompt} fraction) was estimated by varying i) the p_{T}-differential

JHEP10(2018)174

Particle	D^0		D^+		D^{*+}		D_s^+	
0–10% centrality class								
p_T interval (GeV/c)	1–2	7–8	2–3	7–8	3–4	7–8	4–6	6–8
Syst. on dN/dp_T in Pb–Pb	$^{+21}_{-22}$%	$^{+16}_{-17}$%	22%	$^{+16}_{-17}$%	21%	20%	$^{+23}_{-25}$%	$^{+19}_{-23}$%
Yield extraction	15%	5%	12%	7%	11%	7%	6%	6%
Tracking efficiency	6%	7%	8.5%	11%	10%	10%	11%	12%
PID efficiency	0	0	0	0	0	0	3%	3%
Cut efficiency	10%	6%	12%	8%	13%	10%	13%	10%
MC p_T shape	8%	0	10%	0	4%	0	7%	2%
Branching ratio	1.0%	1.0%	2.5%	2.5%	1.3%	1.3%	3.5%	3.5%
Feed-down subtraction	$^{+6.8}_{-7.3}$%	$^{+12.4}_{-12.8}$%	$^{+2.7}_{-3.0}$%	$^{+6.0}_{-6.3}$%	$^{+6.1}_{-6.5}$%	$^{+11.5}_{-11.8}$%	$^{+4.0}_{-9.5}$%	$^{+6.7}_{-14.7}$%
Centrality limit	<0.1%							
Syst. on dN/dp_T in pp and $\sqrt{s}$-scaling of the pp ref.	$^{+8.8}_{-9.0}$%	$^{+8.4}_{-9.4}$%	13%	$^{+8.8}_{-9.1}$%	8.3%	$^{+8.1}_{-8.4}$%	$^{+13}_{-14}$%	$^{+13}_{-14}$%
Syst. on R_{AA}	$^{+22}_{-27}$%	$^{+17}_{-16}$%	$^{+26}_{-27}$%	19%	23%	21%	$^{+27}_{-28}$%	$^{+23}_{-26}$%
60–80% centrality class								
p_T interval (GeV/c)	1–2	7–8	2–3	7–8	1–2	7–8	2–4	6–8
Syst. on dN/dp_T in Pb–Pb	22%	$^{+12}_{-13}$%	12%	13%	23%	14%	23%	20%
Yield extraction	10%	4.5%	4%	3%	13%	2%	10%	6%
Tracking efficiency	6%	7%	8.5%	11%	9%	9%	8.5%	12%
PID efficiency	0	0	0	0	0	0	3%	3%
Cut efficiency	10%	5%	6%	5%	15%	8%	14%	12%
MC p_T shape	12%	0	4%	0	5%	0	6%	2%
Branching ratio	1.0%	1.0%	2.5%	2.5%	1.3%	1.3%	3.5%	3.5%
Feed-down subtraction	$^{+9.0}_{-9.7}$%	$^{+6.1}_{-7.2}$%	$^{+3.0}_{-3.3}$%	$^{+3.8}_{-4.4}$%	$^{+4.4}_{-4.8}$%	$^{+6.4}_{-7.4}$%	$^{+7.2}_{-7.9}$%	$^{+9.2}_{-10.6}$%
Centrality limit	3.0%							
Syst. on dN/dp_T in pp and $\sqrt{s}$-scaling of the pp ref.	$^{+8.8}_{-9.0}$%	$^{+8.4}_{-9.4}$%	13%	$^{+8.8}_{-9.1}$%	12%	$^{+8.1}_{-8.4}$%	13%	$^{+13}_{-14}$%
Syst. on R_{AA}	$^{+23}_{-28}$%	14%	$^{+18}_{-20}$%	16%	$^{+26}_{-31}$%	16%	26%	23%

Table 2. Relative systematic uncertainties on the dN/dp_T in Pb–Pb collisions, on the extrapolated dN/dp_T in pp collisions and on the R_{AA} of D^0, D^{*+}, D^+, and D_s^+ in two centrality classes considered in the analysis for the lowest accessible p_T intervals and for the intermediate range $7 < p_T < 8\,\text{GeV}/c$ ($6 < p_T < 8\,\text{GeV}/c$ for the D_s^+ meson).

JHEP10(2018)174

feed-down D-meson cross section from the FONLL calculation within the theoretical uncertainties, ii) the ratio of the feed-down and prompt D-meson $R_{\rm AA}$ in the ranges described at the end of section 3. The resulting uncertainty ranges between 2% and 15%, depending on D-meson species, centrality classes and $p_{\rm T}$ intervals.

The systematic uncertainties on the $p_{\rm T}$-differential spectra and $R_{\rm AA}$ in the two extreme centrality classes are listed for all D-meson species in table 2 for the lowest $p_{\rm T}$ interval accessible as well as for the intermediate range $7 < p_{\rm T} < 8\,{\rm GeV}/c$ ($6 < p_{\rm T} < 8\,{\rm GeV}/c$ for the $\rm D_s^+$ meson).

The systematic uncertainties on the $R_{\rm AA}$ measurement include those on the D-meson corrected yields described above, those on the proton-proton reference cross section, and the uncertainties on the average nuclear overlap function.

The systematic uncertainty on the pp reference used for the calculation of $R_{\rm AA}$ has two contributions. The first one is the systematic uncertainty on the measured $p_{\rm T}$-differential D-meson cross section at $\sqrt{s} = 7\,{\rm TeV}$. The second contribution is the scaling to $\sqrt{s} = 5.02\,{\rm TeV}$, which has been discussed in section 4.

In the calculation of the nuclear modification factor, the systematic uncertainty on the feed-down subtraction deriving from the variation of the parameters of the FONLL calculation was considered to be correlated in the Pb–Pb and pp measurements, while all the other sources of systematic uncertainties were treated as uncorrelated.

The uncertainties on the $R_{\rm AA}$ normalisation are the quadratic sum of (i) the pp normalisation uncertainty (3.5%), (ii) the uncertainty on $\langle T_{\rm AA} \rangle$, which ranges from 1.9% to 3.4% depending on the centrality, and (iii) the variation of raw yield ($< 0.1\%$, 2% and 3% for the 0–10%, 30–50% and 60–80% centrality classes, respectively) obtained when the centrality intervals are varied to account for the uncertainty on the fraction of the hadronic cross section used in the Glauber fit to determine the centrality [23], and the branching ratio uncertainty cancels out in the ratio.

6 Results

The transverse-momentum distributions ${\rm d}N/{\rm d}p_{\rm T}$ of prompt $\rm D^0$, $\rm D^+$, $\rm D^{*+}$ and $\rm D_s^+$ mesons are shown in figure 3 for the 0–10%, 30–50% and 60–80% centrality classes. The vertical bars represent the statistical uncertainties and the empty boxes the systematic uncertainties. The uncertainty on the branching ratios is quoted separately.

Figure 4 shows the $p_{\rm T}$-dependent ratios of meson yields, $\rm D^+/D^0$, $\rm D^{*+}/D^0$, $\rm D_s^+/D^0$ and $\rm D_s^+/D^+$, compared to the values measured in pp collisions at $\sqrt{s} = 7\,{\rm TeV}$ [40]. The systematic uncertainties were propagated to the ratios, considering the contribution from the tracking efficiency as a fully correlated uncertainty among the four D-meson species. The beauty-hadron feed-down subtraction was considered as fully correlated among the three non-strange D-meson species, while uncorrelated between $\rm D_s^+$ and non-strange D mesons. The $\rm D^+/D^0$ and $\rm D^{*+}/D^0$ ratios are compatible in Pb–Pb and pp collisions, indicating no significant modification of their relative abundances as a function of $p_{\rm T}$ and in centrality classes. The $\rm D_s^+/D^0$ and $\rm D_s^+/D^+$ ratios are measured at $\sqrt{s_{\rm NN}} = 5.02\,{\rm TeV}$ with a precision better by a factor about two with respect to 2.76 TeV [23]. The values of these ratios

JHEP10(2018)174

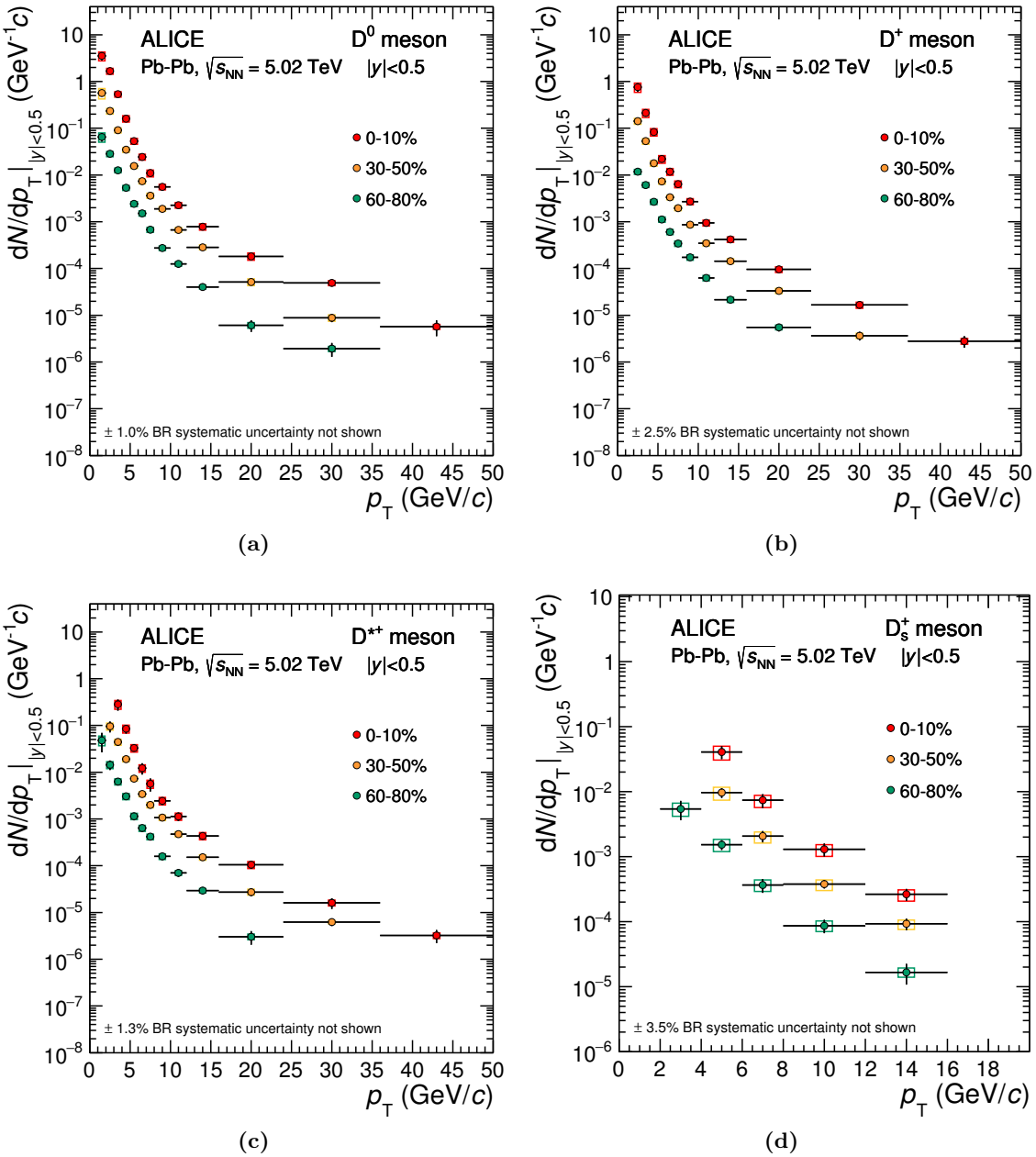

Figure 3. Transverse momentum distributions $\mathrm{d}N/\mathrm{d}p_{\mathrm{T}}$ of prompt D^0 (a), D^+ (b), D^{*+} (c) and $\mathrm{D}_{\mathrm{s}}^+$ (d) mesons in the 0–10%, 30–50% and 60–80% centrality classes in Pb–Pb collisions at $\sqrt{s_{\mathrm{NN}}} = 5.02\,\mathrm{TeV}$. Statistical uncertainties (bars) and systematic uncertainties (boxes) are shown. The uncertainty on the branching ratios is quoted separately. Horizontal bars represent bin widths, symbols are placed at the centre of the bin.

JHEP10(2018)174

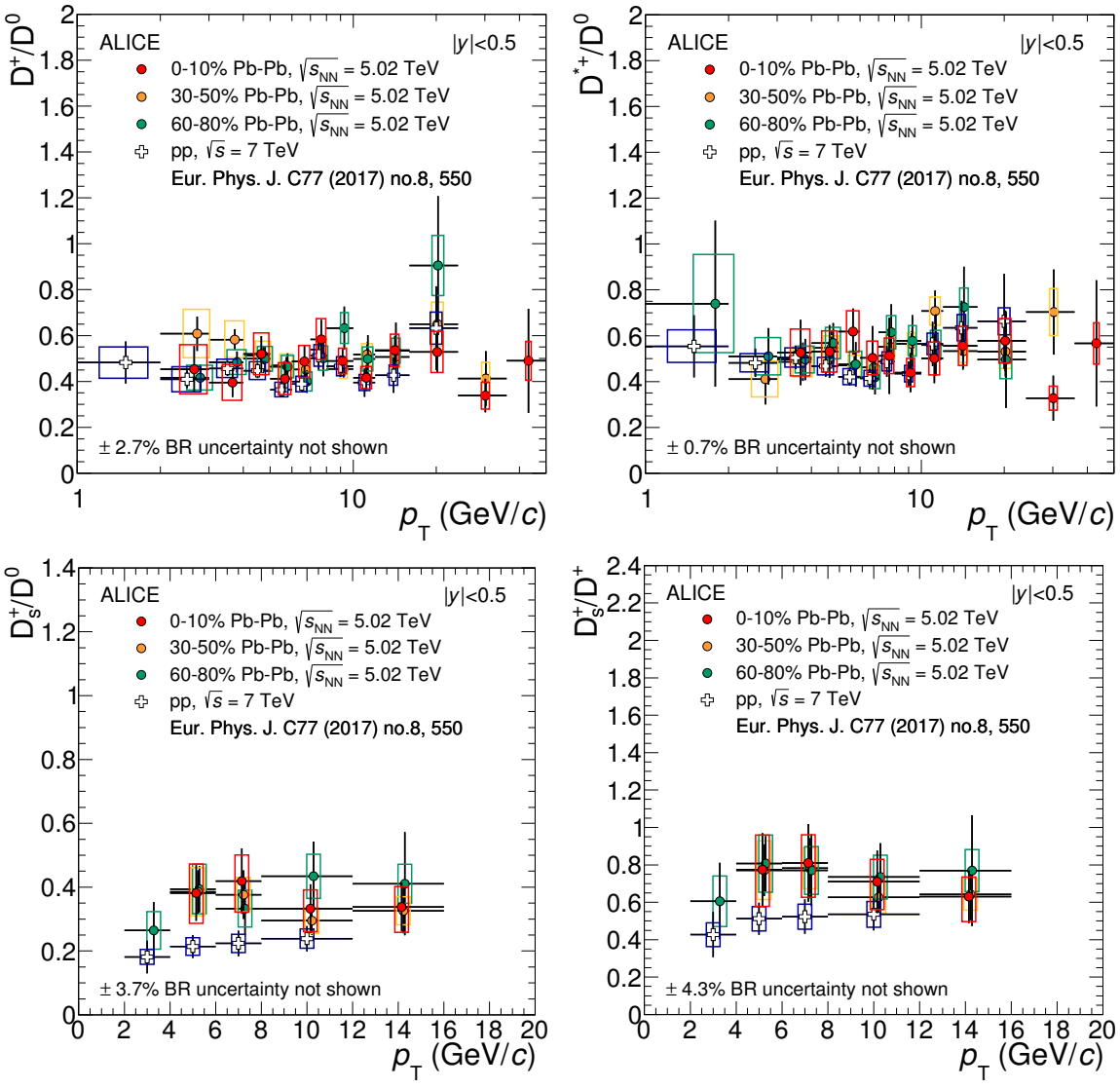

Figure 4. Ratio of prompt D-meson yields as a function of p_{T}. Statistical (bars) and systematic (boxes) uncertainties are shown.

are larger in Pb–Pb than in pp collisions, in all three centrality classes, however the measurements in the two systems are compatible within about one standard deviation of the combined uncertainties.

The R_{AA} of prompt D^0, D^+ and D^{*+} mesons is shown in the left-hand panels of figure 5, from central (top) to peripheral (bottom) collisions. The nuclear modification factors of the three D-meson species are compatible within statistical uncertainties, which are obtained by propagating those on the Pb–Pb yields and those of the pp reference. Their average was computed using the inverse of the quadratic sum of the relative statistical and uncorrelated systematic uncertainties as weights, in the p_{T} intervals where more than one D-meson species is available, (figure 5, right-hand panels). The systematic uncertainties were propagated through the averaging procedure, considering the contributions from the

JHEP10(2018)174

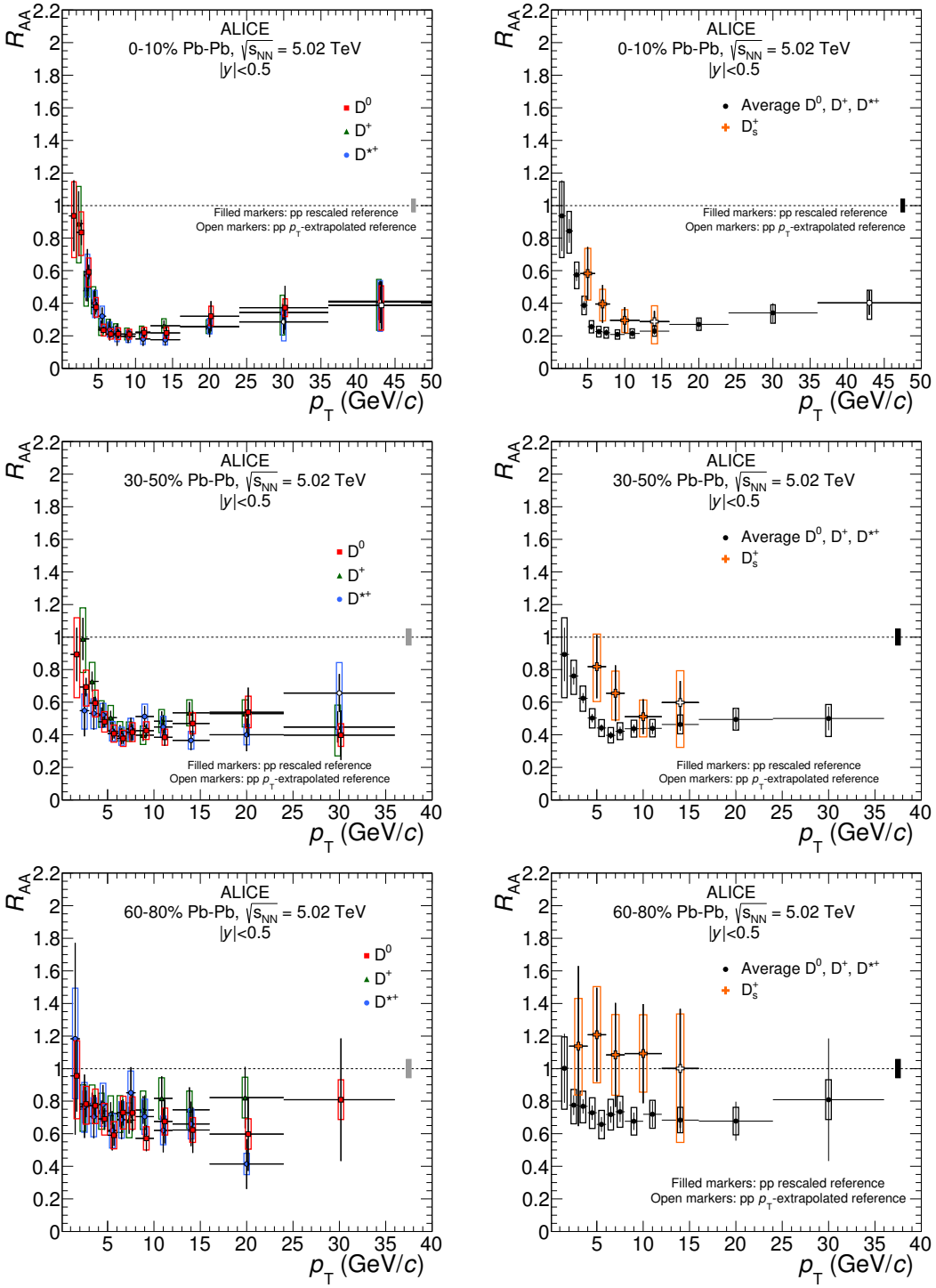

Figure 5. $R_{\rm AA}$ of prompt $\rm D^0$, $\rm D^+$ and $\rm D^{*+}$ mesons (left-hand panels) and of prompt $\rm D_s^+$ mesons compared with the average $R_{\rm AA}$ of the non-strange D-meson states available in each $p_{\rm T}$ interval (right-hand panels) for the 0–10%, 30–50% and 60–80% centrality classes. Statistical (bars), systematic (empty boxes), and normalisation (shaded box around unity) uncertainties are shown. Filled markers are obtained with the pp rescaled reference, empty markers with the $p_{\rm T}$-rescaled reference.

JHEP10(2018)174

tracking efficiency, the beauty-hadron feed-down subtraction and the FONLL-based $\sqrt{s}$-scaling of the pp cross section from $\sqrt{s} = 7\,\text{TeV}$ to $\sqrt{s} = 5.02\,\text{TeV}$ as fully correlated uncertainties among the three D-meson species. The average nuclear modification factors in the 0–10% and 30–50% centrality classes (top and middle right-hand panels of figure 5) show a suppression that is maximal at $p_{\text{T}} = 6$–$10\,\text{GeV}/c$, where a reduction of the yields by a factor of about 5 and 2.5 with respect to the binary-scaled pp reference is observed in the two centrality classes, respectively. The suppression gets smaller with decreasing p_{T} for $p_{\text{T}} < 6\,\text{GeV}/c$, and R_{AA} is compatible with unity in the interval $1 < p_{\text{T}} < 3\,\text{GeV}/c$. The average R_{AA} in the 60–80% centrality class shows a suppression by about 20–30%, without a pronounced dependence on p_{T}.

The R_{AA} of prompt D_s^+ mesons is shown in the right-hand panels of figure 5, where it is compared with the average R_{AA} of non-strange D mesons: the values are larger for D_s^+ mesons, but the two measurements are compatible within one standard deviation of the combined uncertainties, as is the case for the ratios shown in figure 4. The average R_{AA} of prompt D^0, D^+ and D^{*+} in the 10% most central collisions is compared with a measurement of prompt D^0 mesons by the CMS collaboration [26] in the rapidity interval $|y| < 1$ in figure 6 (left panel): the measurements are compatible in the common p_{T} interval 2–50 GeV/c. In the right panel of figure 6, the nuclear modification factor of D mesons at $\sqrt{s_{\text{NN}}} = 5.02\,\text{TeV}$ in the 0–10% centrality class is compared with the same measurement at $\sqrt{s_{\text{NN}}} = 2.76\,\text{TeV}$ [23].[1] The measurement at $\sqrt{s_{\text{NN}}} = 5.02\,\text{TeV}$ have total uncertainties reduced by a factor of about two and extended p_{T} coverage from 36 to $50\,\text{GeV}/c$. The suppression is compatible within uncertainties at the two energies, as also observed for charged particles [59].

The close similarity of the R_{AA} measurements at the two energies was predicted by the Djordjevic model [54] (figure 6, right panel), and it results from the combination of a higher medium temperature at 5.02 TeV (estimated to be about 7% higher than at 2.76 TeV), which would decrease the R_{AA} by about 10%, with a harder p_{T} distribution of charm quarks at 5.02 TeV, which would increase the R_{AA} by about 5% if the medium temperature were the same as at 2.76 TeV.

As explained in section 1, the measurement of the R_{AA} of open-charm mesons is essential to understand in-medium parton energy loss, in particular its colour-charge and quark-mass dependence. In figure 7, the R_{AA} of prompt D mesons is compared with that of charged particles in the same p_{T} intervals, at the same energy and in the same centrality classes [59]. The ratio of their nuclear modification factors is displayed in the bottom panels, for the three centrality classes. The R_{AA} of D mesons and charged particles differ by more than $2\,\sigma$ of the combined statistical and systematic uncertainties in all the p_{T} intervals within $3 < p_{\text{T}} < 8\,\text{GeV}/c$ in central collisions. The difference is less than $2\,\sigma$ in this range for semi-central collisions, while the two R_{AA} are the same within $1\,\sigma$ for $p_{\text{T}} > 10\,\text{GeV}/c$ in both central and semi-central collisions. In the 60–80% class the measurements are compatible in the common p_{T} interval. The interpretation of the difference observed for

[1] The T_{AA} used to compute the D-meson R_{AA} at $\sqrt{s_{\text{NN}}} = 2.76\,\text{TeV}$ in the 0–10% centrality class and its uncertainty were updated with respect to [23] according to the values reported in ref. [36].

JHEP10(2018)174

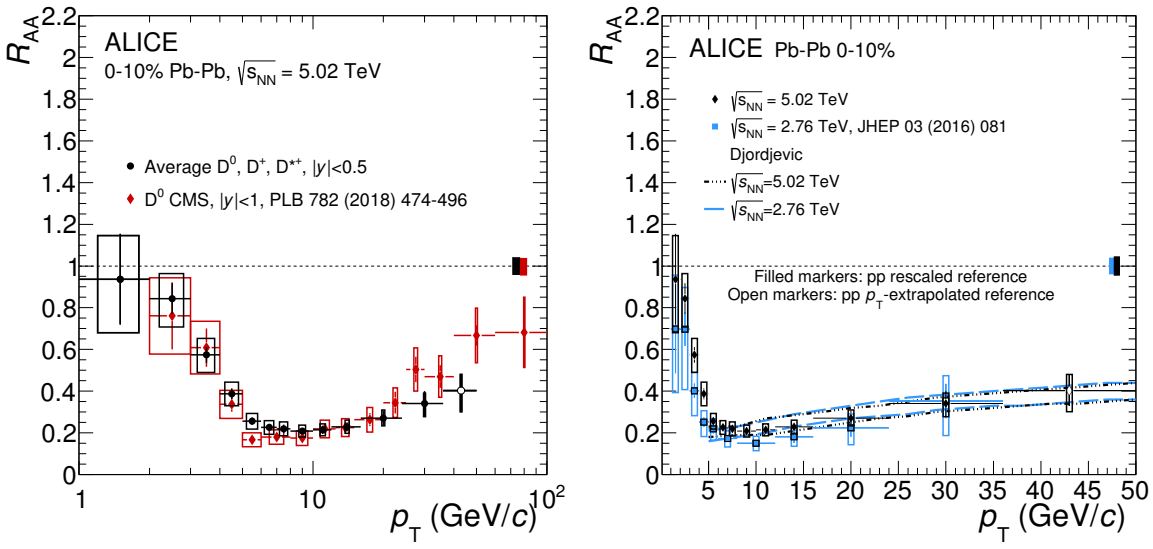

Figure 6. Left panel: average $R_{\rm AA}$ of prompt $\rm D^0$, $\rm D^+$ and $\rm D^{*+}$ mesons by ALICE compared to $R_{\rm AA}$ of prompt $\rm D^0$ mesons by CMS [26] in the 0–10% centrality class and at $\sqrt{s_{\rm NN}} = 5.02\,\text{TeV}$. Statistical (bars), systematic (empty boxes), and normalisation (shaded box around unity) uncertainties are shown. Right panel: average $R_{\rm AA}$ of $\rm D^0$, $\rm D^+$ and $\rm D^{*+}$ mesons compared with the Djordjevic model [54] in the 0–10% centrality class at two collision energies. Statistical (bars), systematic (empty boxes), and normalisation (shaded box) uncertainties are shown.

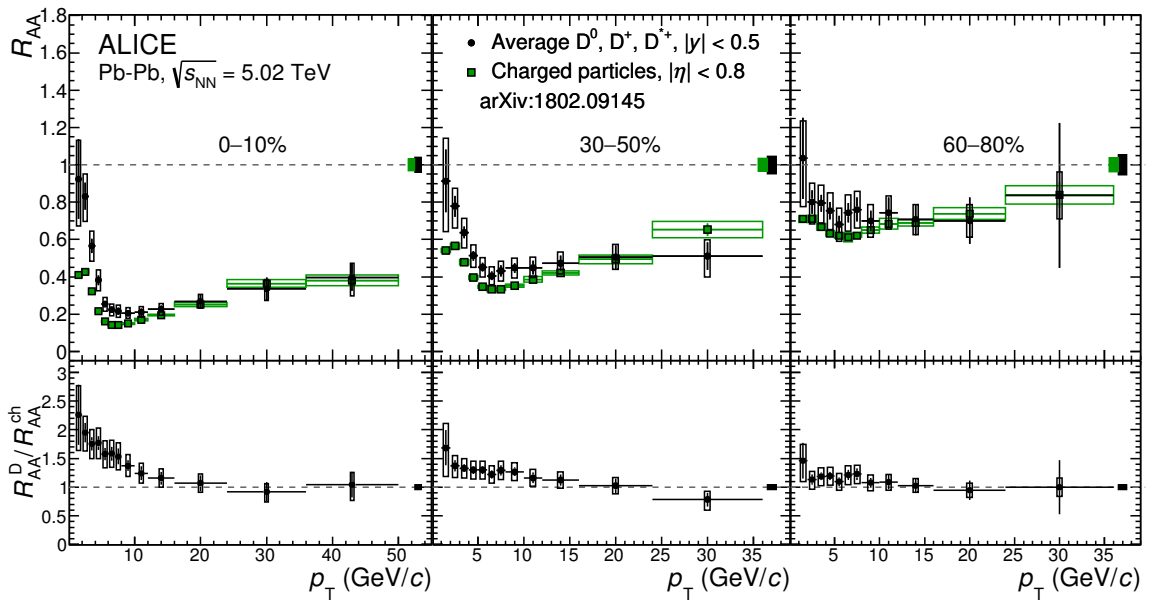

Figure 7. Average $R_{\rm AA}$ of prompt $\rm D^0$, $\rm D^+$ and $\rm D^{*+}$ mesons in the 0–10% (left), 30–50% (middle) and 60–80% (right) centrality classes at $\sqrt{s_{\rm NN}} = 5.02\,\text{TeV}$ compared to the $R_{\rm AA}$ of charged particles in the same centrality classes [59]. The ratios of the $R_{\rm AA}$ are shown in the bottom panels. Statistical (bars), systematic (empty boxes), and normalisation (shaded box around unity) uncertainties are shown.

JHEP10(2018)174

$p_{\rm T} < 8\,{\rm GeV}/c$ in central and semi-central collisions is not straightforward, because several factors can play a role in defining the shape of the $R_{\rm AA}$.

In presence of a colour-charge and quark-mass dependent energy loss, the harder $p_{\rm T}$ distribution and the harder fragmentation function of charm quarks compared to those of light quarks and gluons should lead to similar values of D-meson and pion $R_{\rm AA}$, as discussed in [60]. Since the pions are the dominant contribution in the inclusive charged-particle yields, this statement is expected to be still valid for the comparison of the D-meson and the charged particle $R_{\rm AA}$. In addition, it should be considered that the yield of light-flavour hadrons could have a substantial contribution up to transverse momenta of about 2–3 GeV/c from soft production processes, such as the break-down of participant nucleons into quarks and gluons that subsequently hadronise. This component scales with the number of participants rather than the number of binary collisions. Finally, the effects of radial flow and hadronisation via recombination, as well as initial-state effects, could affect D-meson and light-hadron yields differently at a given $p_{\rm T}$.

The average $R_{\rm AA}$ of the three non-strange D-meson species in the three centrality classes are compared with theoretical models in figure 8. Models based on heavy-quark transport and models based on perturbative QCD calculations of high-$p_{\rm T}$ parton energy loss are shown in the left and in the right panels, respectively. Transport models in the left panels include: BAMPS el. [57], POWLANG [61] and TAMU [55], in which the interactions are only described by collisional (i.e. elastic) processes; BAMPS el.+rad. [57], LBT [58], MC@sHQ+EPOS2 [62] and PHSD [63], in which also energy loss from medium-induced gluon radiation is considered, in addition to collisional process. In the right panels, the CUJET3.0 [64] and Djordjevic [54] models include both radiative and collisional energy loss processes, while the SCET [65] model implements medium-induced gluon radiation via modified splitting functions with finite quark masses.[2] All models, with the exception of BAMPS and CUJET3.0, include a nuclear modification of the parton distribution functions. The LBT, MC@sHQ, PHSD, POWLANG and TAMU models include a contribution of hadronisation via quark recombination, in addition to independent fragmentation. Most of the models provide a fair description of the data in the region $p_{\rm T} < 10\,{\rm GeV}/c$ in central collisions (except for BAMPS el., where the radiative term is missing), but many of them (LBT, PHSD, POWLANG and SCET) provide a worse description of non-central collisions. In the high-$p_{\rm T}$ region above 10 GeV/c only the BAMPS el.+rad., CUJET3.0, Djordjevic, MC@sHQ+EPOS2 and SCET models can describe the data in central collisions. The CUJET3.0 and Djordjevic models provide a fair description of the $R_{\rm AA}$ in all three centrality classes for $p_{\rm T} > 10\,{\rm GeV}/c$, where radiative energy loss is expected to be the dominant interaction mechanism, suggesting that the dependence of radiative energy loss on the path length in the hot and dense medium is well understood.

In figure 9, the non-strange and strange D-meson $R_{\rm AA}$ are compared with the models that provide both observables. An increase of the $\rm D_s^+$ $R_{\rm AA}$ is expected in the two models, PHSD and TAMU, in particular for $p_{\rm T} < 5\,{\rm GeV}/c$, with respect to non-strange D mesons.

[2]The SCET curves reported here differ from those of ref. [65] because the latter used an extrapolation of the charged-particle multiplicity at $\sqrt{s_{\rm NN}} = 5.02\,{\rm TeV}$, while now the measured values are used.

JHEP10(2018)174

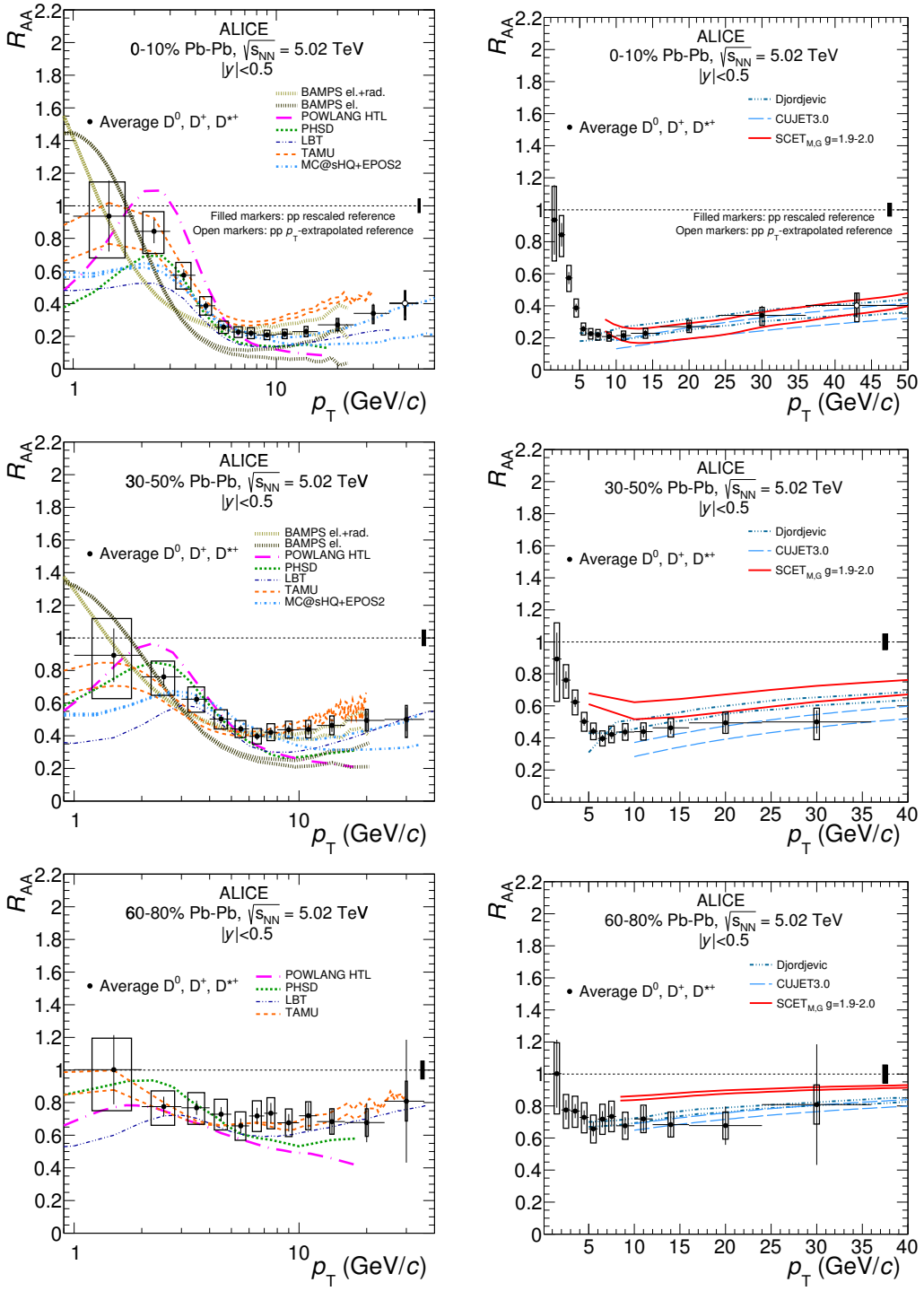

Figure 8. Average $R_{\rm AA}$ of $\rm D^0$, $\rm D^+$ and $\rm D^{*+}$ mesons compared with model calculations. The three rows refer to the 0–10%, 30–50% and 60–80% centrality classes. The left panels show models based on heavy-quark transport, while the right panels show models based on pQCD energy loss. Model nomenclature and references: BAMPS [57], CUJET3.0 [64], Djordjevic [54], LBT [58], MC@sHQ+EPOS2 [62], PHSD [63] POWLANG [61], SCET [65], TAMU [55]. Some of the models are presented with two lines with the same style and colour, which encompass the model uncertainty band.

JHEP10(2018)174

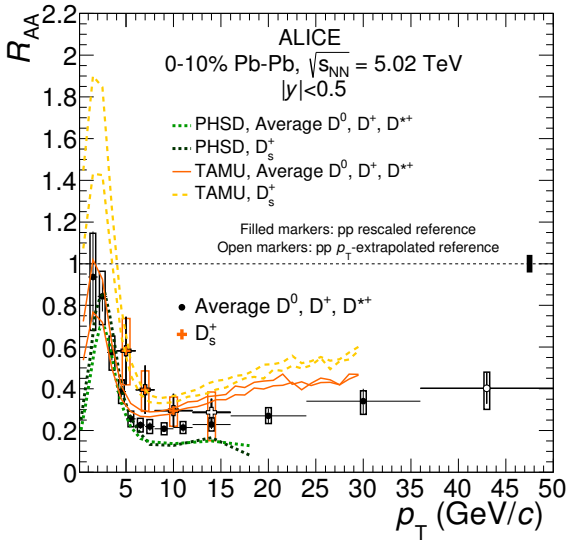

Figure 9. Average $R_{\rm AA}$ of $\rm D^0$, $\rm D^+$ and $\rm D^{*+}$ mesons and $R_{\rm AA}$ of $\rm D_s^+$ mesons in the 0–10% centrality class compared with the PHSD [63] and TAMU [55] model calculations.

This increase is induced by hadronisation via quark recombination in the QGP, as well as by different interaction cross sections for non-strange D and for $\rm D_s^+$ in the hadronic phase of the system evolution. In the transverse momentum interval covered by the $\rm D_s^+$ measurement ($p_{\rm T} > 4\,{\rm GeV}/c$), the PHSD model predicts the effect to be very small, while the TAMU model predicts a sizeable difference of about 30% up to about $8\,{\rm GeV}/c$, similar to the trend shown by the data.

The simultaneous comparison of $R_{\rm AA}$ and elliptic flow v_2 measurements at $\sqrt{s_{\rm NN}} = 5.02\,{\rm TeV}$ [66] with models can provide more stringent constraints to the implementation of the interaction and hadronisation processes for heavy quarks in the QGP. The comparison with models that compute both observables is shown in figure 10 for the $R_{\rm AA}$ and v_2, in the 0–10% and 30–50% centrality classes, respectively. The TAMU model overestimates $R_{\rm AA}$ and underestimates v_2 at high $p_{\rm T}$, probably because it does not include radiative energy loss. The BAMPS el. model overestimates the maximum flow while underestimating the $R_{\rm AA}$ value at high $p_{\rm T}$. The radiative energy loss contribution in BAMPS el.+rad. improves the description of $R_{\rm AA}$ but gives v_2 values lower than the data. The LBT, PHSD, POWLANG and MC@sHQ models provide instead a fair description of v_2. Nevertheless, energy loss is overestimated at high $p_{\rm T}$ in the 0–10% centrality classes (but also in semi-central events) by PHSD, POWLANG and LBT, while at low $p_{\rm T}$ the measured $R_{\rm AA}$ is slightly higher than what predicted within LBT, PHSD and MC@sHQ.

7 Summary

We have presented measurements of the $p_{\rm T}$-differential production yields of prompt $\rm D^0$, $\rm D^+$, $\rm D^{*+}$ and $\rm D_s^+$ mesons at central rapidity in Pb–Pb collisions in the three centrality classes 0–10%, 30–50% and 60–80% at a centre-of-mass energy per nucleon pair $\sqrt{s_{\rm NN}} = 5.02\,{\rm TeV}$.

JHEP10(2018)174

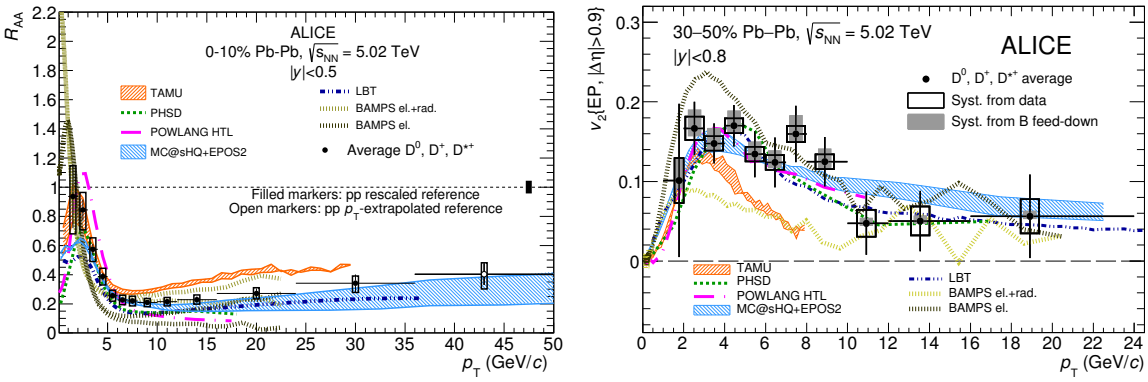

Figure 10. Average $R_{\rm AA}$ of $\rm D^0$, $\rm D^+$ and $\rm D^{*+}$ mesons in the 0–10% centrality class (left) and their average elliptic flow v_2 in the 30–50% centrality class (right) [66], compared with models that have predictions for both observables at low $p_{\rm T}$.

The average $R_{\rm AA}$ of the three non-strange D-meson species shows minimum values of 0.2 and 0.4 in the centrality classes 0–10% and 30–50%, respectively, at $p_{\rm T}$ of 6–10 GeV/c. $R_{\rm AA}$ increases for $p_{\rm T} < 6$ GeV/c, and it is compatible with unity at $1 < p_{\rm T} < 3$ GeV/c. The average $R_{\rm AA}$ values are compatible with those measured at $\sqrt{s_{\rm NN}} = 2.76$ TeV and they have smaller uncertainties by a factor of about two, as well as extended $p_{\rm T}$ coverage up to 50 GeV/c in central collisions. The similarity of the $R_{\rm AA}$ values at the two energies was predicted by the Djordjevic model, and it results from the combination of a higher medium temperature at 5.02 TeV (estimated to be about 7% higher than at 2.76 TeV) with a harder $p_{\rm T}$ distribution of charm quarks at 5.02 TeV.

In central and semi-central collisions the average $R_{\rm AA}$ of non-strange D mesons is compatible with that of charged particles for $p_{\rm T} > 6$ GeV/c, while it is larger at lower $p_{\rm T}$. The $R_{\rm AA}$ of $\rm D_s^+$ mesons have generally larger central values than those of the average of non-strange D mesons, but the two measurements are compatible within about one standard deviation of the combined uncertainties.

The $R_{\rm AA}$ of non-strange D mesons at high $p_{\rm T}$ (above 10 GeV/c) is fairly described in the three centrality classes by model calculations that include both radiative and collisional energy loss. This indicates that the centrality dependence of radiative energy loss, which is the dominant contribution at high $p_{\rm T}$, is under good theoretical control. The $R_{\rm AA}$ in the transverse momentum region below 10 GeV/c is described by several transport model calculations in central collisions, but most models fail in describing the centrality dependence of $R_{\rm AA}$ and in describing simultaneously $R_{\rm AA}$ and the elliptic flow coefficient v_2. Therefore, the measurements provide significant constraints for the understanding of the interaction of charm quarks with the high-density QCD medium, especially at low and intermediate $p_{\rm T}$, where the $R_{\rm AA}$ is the result of a more complex interplay among several effects.

Acknowledgments

The ALICE collaboration would like to thank all its engineers and technicians for their invaluable contributions to the construction of the experiment and the CERN accelerator

JHEP10(2018)174

teams for the outstanding performance of the LHC complex. The ALICE collaboration gratefully acknowledges the resources and support provided by all Grid centres and the Worldwide LHC Computing Grid (WLCG) collaboration. The ALICE collaboration acknowledges the following funding agencies for their support in building and running the ALICE detector: A.I. Alikhanyan National Science Laboratory (Yerevan Physics Institute) Foundation (ANSL), State Committee of Science and World Federation of Scientists (WFS), Armenia; Austrian Academy of Sciences and Nationalstiftung für Forschung, Technologie und Entwicklung, Austria; Ministry of Communications and High Technologies, National Nuclear Research Center, Azerbaijan; Conselho Nacional de Desenvolvimento Científico e Tecnológico (CNPq), Universidade Federal do Rio Grande do Sul (UFRGS), Financiadora de Estudos e Projetos (Finep) and Fundação de Amparo à Pesquisa do Estado de São Paulo (FAPESP), Brazil; Ministry of Science & Technology of China (MSTC), National Natural Science Foundation of China (NSFC) and Ministry of Education of China (MOEC), China; Ministry of Science and Education, Croatia; Ministry of Education, Youth and Sports of the Czech Republic, Czech Republic; The Danish Council for Independent Research — Natural Sciences, the Carlsberg Foundation and Danish National Research Foundation (DNRF), Denmark; Helsinki Institute of Physics (HIP), Finland; Commissariat à l'Energie Atomique (CEA) and Institut National de Physique Nucléaire et de Physique des Particules (IN2P3) and Centre National de la Recherche Scientifique (CNRS), France; Bundesministerium für Bildung, Wissenschaft, Forschung und Technologie (BMBF) and GSI Helmholtzzentrum für Schwerionenforschung GmbH, Germany; General Secretariat for Research and Technology, Ministry of Education, Research and Religions, Greece; National Research, Development and Innovation Office, Hungary; Department of Atomic Energy Government of India (DAE), Department of Science and Technology, Government of India (DST), University Grants Commission, Government of India (UGC) and Council of Scientific and Industrial Research (CSIR), India; Indonesian Institute of Science, Indonesia; Centro Fermi — Museo Storico della Fisica e Centro Studi e Ricerche Enrico Fermi and Istituto Nazionale di Fisica Nucleare (INFN), Italy; Institute for Innovative Science and Technology, Nagasaki Institute of Applied Science (IIST), Japan Society for the Promotion of Science (JSPS) KAKENHI and Japanese Ministry of Education, Culture, Sports, Science and Technology (MEXT), Japan; Consejo Nacional de Ciencia (CONACYT) y Tecnología, through Fondo de Cooperación Internacional en Ciencia y Tecnología (FONCICYT) and Dirección General de Asuntos del Personal Academico (DGAPA), Mexico; Nederlandse Organisatie voor Wetenschappelijk Onderzoek (NWO), Netherlands; The Research Council of Norway, Norway; Commission on Science and Technology for Sustainable Development in the South (COMSATS), Pakistan; Pontificia Universidad Católica del Perú, Peru; Ministry of Science and Higher Education and National Science Centre, Poland; Korea Institute of Science and Technology Information and National Research Foundation of Korea (NRF), Republic of Korea; Ministry of Education and Scientific Research, Institute of Atomic Physics and Romanian National Agency for Science, Technology and Innovation, Romania; Joint Institute for Nuclear Research (JINR), Ministry of Education and Science of the Russian Federation and National Research Centre Kurchatov Institute, Russia; Ministry of Education, Science, Research and Sport of the Slovak Republic, Slovakia; National

JHEP10(2018)174

Research Foundation of South Africa, South Africa; Centro de Aplicaciones Tecnológicas y Desarrollo Nuclear (CEADEN), Cubaenergía, Cuba and Centro de Investigaciones Energéticas, Medioambientales y Tecnológicas (CIEMAT), Spain; Swedish Research Council (VR) and Knut & Alice Wallenberg Foundation (KAW), Sweden; European Organization for Nuclear Research, Switzerland; National Science and Technology Development Agency (NSDTA), Suranaree University of Technology (SUT) and Office of the Higher Education Commission under NRU project of Thailand, Thailand; Turkish Atomic Energy Agency (TAEK), Turkey; National Academy of Sciences of Ukraine, Ukraine; Science and Technology Facilities Council (STFC), United Kingdom; National Science Foundation of the United States of America (NSF) and United States Department of Energy, Office of Nuclear Physics (DOE NP), United States of America.

Open Access. This article is distributed under the terms of the Creative Commons Attribution License (CC-BY 4.0), which permits any use, distribution and reproduction in any medium, provided the original author(s) and source are credited.

References

[1] F. Karsch, *Lattice simulations of the thermodynamics of strongly interacting elementary particles and the exploration of new phases of matter in relativistic heavy ion collisions*, *J. Phys. Conf. Ser.* **46** (2006) 122 [hep-lat/0608003] [INSPIRE].

[2] WUPPERTAL-BUDAPEST collaboration, S. Borsányi et al., *Is there still any T_c mystery in lattice QCD? Results with physical masses in the continuum limit III*, *JHEP* **09** (2010) 073 [arXiv:1005.3508] [INSPIRE].

[3] S. Borsányi, Z. Fodor, C. Hölbling, S.D. Katz, S. Krieg and K.K. Szabo, *Full result for the QCD equation of state with $2+1$ flavors*, *Phys. Lett.* **B 730** (2014) 99 [arXiv:1309.5258] [INSPIRE].

[4] A. Bazavov et al., *The chiral and deconfinement aspects of the QCD transition*, *Phys. Rev.* **D 85** (2012) 054503 [arXiv:1111.1710] [INSPIRE].

[5] A. Andronic et al., *Heavy-flavour and quarkonium production in the LHC era: from proton-proton to heavy-ion collisions*, *Eur. Phys. J.* **C 76** (2016) 107 [arXiv:1506.03981] [INSPIRE].

[6] F.-M. Liu and S.-X. Liu, *Quark-gluon plasma formation time and direct photons from heavy ion collisions*, *Phys. Rev.* **C 89** (2014) 034906 [arXiv:1212.6587] [INSPIRE].

[7] P. Braun-Munzinger, *Quarkonium production in ultra-relativistic nuclear collisions: Suppression versus enhancement*, *J. Phys.* **G 34** (2007) S471 [nucl-th/0701093] [INSPIRE].

[8] M. Gyulassy and M. Plumer, *Jet Quenching in Dense Matter*, *Phys. Lett.* **B 243** (1990) 432 [INSPIRE].

[9] R. Baier, Y.L. Dokshitzer, A.H. Mueller, S. Peigne and D. Schiff, *Radiative energy loss and p_T broadening of high-energy partons in nuclei*, *Nucl. Phys.* **B 484** (1997) 265 [hep-ph/9608322] [INSPIRE].

[10] M.H. Thoma and M. Gyulassy, *Quark Damping and Energy Loss in the High Temperature QCD*, *Nucl. Phys.* **B 351** (1991) 491 [INSPIRE].

JHEP10(2018)174

[11] E. Braaten and M.H. Thoma, *Energy loss of a heavy fermion in a hot plasma*, *Phys. Rev.* **D 44** (1991) 1298 [INSPIRE].

[12] E. Braaten and M.H. Thoma, *Energy loss of a heavy quark in the quark-gluon plasma*, *Phys. Rev.* **D 44** (1991) R2625 [INSPIRE].

[13] F. Prino and R. Rapp, *Open Heavy Flavor in QCD Matter and in Nuclear Collisions*, *J. Phys.* **G 43** (2016) 093002 [arXiv:1603.00529] [INSPIRE].

[14] S. Batsouli, S. Kelly, M. Gyulassy and J.L. Nagle, *Does the charm flow at RHIC?*, *Phys. Lett.* **B 557** (2003) 26 [nucl-th/0212068] [INSPIRE].

[15] V. Greco, C.M. Ko and R. Rapp, *Quark coalescence for charmed mesons in ultrarelativistic heavy ion collisions*, *Phys. Lett.* **B 595** (2004) 202 [nucl-th/0312100] [INSPIRE].

[16] A. Andronic, P. Braun-Munzinger, K. Redlich and J. Stachel, *Statistical hadronization of charm in heavy ion collisions at SPS, RHIC and LHC*, *Phys. Lett.* **B 571** (2003) 36 [nucl-th/0303036] [INSPIRE].

[17] I. Kuznetsova and J. Rafelski, *Charmed hadrons from strangeness-rich QGP*, *J. Phys.* **G 32** (2006) S499 [hep-ph/0605307] [INSPIRE].

[18] R.J. Glauber and G. Matthiae, *High-energy scattering of protons by nuclei*, *Nucl. Phys.* **B 21** (1970) 135 [INSPIRE].

[19] M.L. Miller, K. Reygers, S.J. Sanders and P. Steinberg, *Glauber modeling in high energy nuclear collisions*, *Ann. Rev. Nucl. Part. Sci.* **57** (2007) 205 [nucl-ex/0701025] [INSPIRE].

[20] B. Alver, M. Baker, C. Loizides and P. Steinberg, *The PHOBOS Glauber Monte Carlo*, arXiv:0805.4411 [INSPIRE].

[21] C. Loizides, J. Nagle and P. Steinberg, *Improved version of the PHOBOS Glauber Monte Carlo*, *SoftwareX* **1–2** (2015) 13 [arXiv:1408.2549] [INSPIRE].

[22] ALICE collaboration, *Suppression of high transverse momentum D mesons in central Pb-Pb collisions at* $\sqrt{s_{\rm NN}} = 2.76$ *TeV*, *JHEP* **09** (2012) 112 [arXiv:1203.2160] [INSPIRE].

[23] ALICE collaboration, *Transverse momentum dependence of D-meson production in Pb-Pb collisions at* $\sqrt{s}_{\rm NN} = 2.76$ *TeV*, *JHEP* **03** (2016) 081 [arXiv:1509.06888] [INSPIRE].

[24] ALICE collaboration, *Centrality dependence of high-*p_T *D meson suppression in Pb-Pb collisions at* $\sqrt{s_{\rm NN}} = 2.76$ *TeV*, *JHEP* **11** (2015) 205 [arXiv:1506.06604] [INSPIRE].

[25] ALICE collaboration, *Measurement of* D_s^+ *production and nuclear modification factor in Pb-Pb collisions at* $\sqrt{s_{\rm NN}} = 2.76$ *TeV*, *JHEP* **03** (2016) 082 [arXiv:1509.07287] [INSPIRE].

[26] CMS collaboration, *Nuclear modification factor of* D^0 *mesons in PbPb collisions at* $\sqrt{s_{\rm NN}} = 5.02$ *TeV*, *Phys. Lett.* **B 782** (2018) 474 [arXiv:1708.04962] [INSPIRE].

[27] ALICE collaboration, *D-meson production in p-Pb collisions at* $\sqrt{s_{\rm NN}} = 5.02$ *TeV and in pp collisions at* $\sqrt{s} = 7$ *TeV*, *Phys. Rev.* **C 94** (2016) 054908 [arXiv:1605.07569] [INSPIRE].

[28] ALICE collaboration, *The ALICE experiment at the CERN LHC*, 2008 *JINST* **3** S08002 [INSPIRE].

[29] ALICE collaboration, *Performance of the ALICE Experiment at the CERN LHC*, *Int. J. Mod. Phys.* **A 29** (2014) 1430044 [arXiv:1402.4476] [INSPIRE].

[30] ALICE collaboration, *Alignment of the ALICE Inner Tracking System with cosmic-ray tracks*, 2010 *JINST* **5** P03003 [arXiv:1001.0502] [INSPIRE].

JHEP10(2018)174

[31] J. Alme et al., *The ALICE TPC, a large 3-dimensional tracking device with fast readout for ultra-high multiplicity events*, *Nucl. Instrum. Meth.* **A 622** (2010) 316 [arXiv:1001.1950] [INSPIRE].

[32] A. Akindinov et al., *Performance of the ALICE Time-Of-Flight detector at the LHC*, *Eur. Phys. J. Plus* **128** (2013) 44 [INSPIRE].

[33] G. Puddu et al., *The Zero degree calorimeters for the ALICE experiment*, *Nucl. Instrum. Meth.* **A 581** (2007) 397 [*Erratum ibid.* **A 604** (2009) 765] [INSPIRE].

[34] ALICE collaboration, *Performance of the ALICE VZERO system*, 2013 *JINST* **8** P10016 [arXiv:1306.3130] [INSPIRE].

[35] ALICE collaboration, *Centrality determination of Pb-Pb collisions at* $\sqrt{s_{\rm NN}} = 2.76$ *TeV with ALICE*, *Phys. Rev.* **C 88** (2013) 044909 [arXiv:1301.4361] [INSPIRE].

[36] ALICE collaboration, *Centrality determination in heavy ion collisions*, ALICE-PUBLIC-2018-011 (2018).

[37] ALICE collaboration, *Centrality dependence of the charged-particle multiplicity density at midrapidity in Pb-Pb collisions at* $\sqrt{s_{\rm NN}} = 5.02$ *TeV*, *Phys. Rev. Lett.* **116** (2016) 222302 [arXiv:1512.06104] [INSPIRE].

[38] Particle Data Group collaboration, C. Patrignani et al., *Review of Particle Physics*, *Chin. Phys.* **C 40** (2016) 100001 [INSPIRE].

[39] ALICE collaboration, *Azimuthal anisotropy of D meson production in Pb-Pb collisions at* $\sqrt{s_{\rm NN}} = 2.76$ *TeV*, *Phys. Rev.* **C 90** (2014) 034904 [arXiv:1405.2001] [INSPIRE].

[40] ALICE collaboration, *Measurement of D-meson production at mid-rapidity in pp collisions at* $\sqrt{s} = 7$ *TeV*, *Eur. Phys. J.* **C 77** (2017) 550 [arXiv:1702.00766] [INSPIRE].

[41] ALICE collaboration, *Measurement of charm production at central rapidity in proton-proton collisions at* $\sqrt{s} = 7$ *TeV*, *JHEP* **01** (2012) 128 [arXiv:1111.1553] [INSPIRE].

[42] P.Z. Skands, *The Perugia Tunes*, in proceedings of the *1st International Workshop on Multiple Partonic Interactions at the LHC (MPI@LHC 08)*, Perugia, Italy, 27–31 October 2008, pp. 284–297 [arXiv:0905.3418] [FERMILAB-CONF-09-113-T] [INSPIRE].

[43] CMS collaboration, *Suppression and azimuthal anisotropy of prompt and nonprompt* J/ψ *production in PbPb collisions at* $\sqrt{s_{\rm NN}} = 2.76$ *TeV*, *Eur. Phys. J.* **C 77** (2017) 252 [arXiv:1610.00613] [INSPIRE].

[44] R. Brun et al., *GEANT Detector Description and Simulation Tool*, CERN-W-5013 (1994) https://doi.org/10.17181/CERN.MUHF.DMJ1 [INSPIRE].

[45] X.-N. Wang and M. Gyulassy, *HIJING: A Monte Carlo model for multiple jet production in pp, pA and AA collisions*, *Phys. Rev.* **D 44** (1991) 3501 [INSPIRE].

[46] T. Sjöstrand, S. Mrenna and P.Z. Skands, *PYTHIA 6.4 Physics and Manual*, *JHEP* **05** (2006) 026 [hep-ph/0603175] [INSPIRE].

[47] M. Cacciari, M. Greco and P. Nason, *The* p_T *spectrum in heavy flavor hadroproduction*, *JHEP* **05** (1998) 007 [hep-ph/9803400] [INSPIRE].

[48] M. Cacciari, S. Frixione and P. Nason, *The* p_T *spectrum in heavy flavor photoproduction*, *JHEP* **03** (2001) 006 [hep-ph/0102134] [INSPIRE].

JHEP10(2018)174

[49] J. Uphoff, O. Fochler, Z. Xu and C. Greiner, *Elliptic Flow and Energy Loss of Heavy Quarks in Ultra-Relativistic heavy Ion Collisions*, *Phys. Rev.* **C 84** (2011) 024908 [arXiv:1104.2295] [INSPIRE].

[50] O. Fochler, J. Uphoff, Z. Xu and C. Greiner, *Jet quenching and elliptic flow at RHIC and LHC within a pQCD-based partonic transport model*, *J. Phys.* **G 38** (2011) 124152 [arXiv:1107.0130] [INSPIRE].

[51] J. Uphoff, O. Fochler, Z. Xu and C. Greiner, *Open Heavy Flavor in $Pb+Pb$ Collisions at $\sqrt{s}=2.76$ TeV within a Transport Model*, *Phys. Lett.* **B 717** (2012) 430 [arXiv:1205.4945] [INSPIRE].

[52] M. Cacciari, S. Frixione, N. Houdeau, M.L. Mangano, P. Nason and G. Ridolfi, *Theoretical predictions for charm and bottom production at the LHC*, *JHEP* **10** (2012) 137 [arXiv:1205.6344] [INSPIRE].

[53] D.J. Lange, *The EvtGen particle decay simulation package*, in proceedings of the *7th International Conference on B-Physics at Hadron Machines (Beauty 2000)*, Sea of Galilee, Kibbutz Maagan, Israel, 13–18 September 2000, *Nucl. Instrum. Meth.* **A 462** (2001) 152 [INSPIRE].

[54] M. Djordjevic and M. Djordjevic, *Predictions of heavy-flavor suppression at 5.1 TeV $Pb+Pb$ collisions at the CERN Large Hadron Collider*, *Phys. Rev.* **C 92** (2015) 024918 [arXiv:1505.04316] [INSPIRE].

[55] M. He, R.J. Fries and R. Rapp, *Heavy Flavor at the Large Hadron Collider in a Strong Coupling Approach*, *Phys. Lett.* **B 735** (2014) 445 [arXiv:1401.3817] [INSPIRE].

[56] R. Averbeck, N. Bastid, Z.C. del Valle, P. Crochet, A. Dainese and X. Zhang, *Reference Heavy Flavour Cross Sections in pp Collisions at $\sqrt{s}=2.76$ TeV, using a pQCD-Driven $\sqrt{s}$-Scaling of ALICE Measurements at $\sqrt{s}=7$ TeV*, arXiv:1107.3243 [INSPIRE].

[57] J. Uphoff, O. Fochler, Z. Xu and C. Greiner, *Elastic and radiative heavy quark interactions in ultra-relativistic heavy-ion collisions*, *J. Phys.* **G 42** (2015) 115106 [arXiv:1408.2964] [INSPIRE].

[58] S. Cao, T. Luo, G.-Y. Qin and X.-N. Wang, *Heavy and light flavor jet quenching at RHIC and LHC energies*, *Phys. Lett.* **B 777** (2018) 255 [arXiv:1703.00822] [INSPIRE].

[59] ALICE collaboration, *Transverse momentum spectra and nuclear modification factors of charged particles in pp, p-Pb and Pb-Pb collisions at the LHC*, arXiv:1802.09145 [INSPIRE].

[60] M. Djordjevic, *Heavy flavor puzzle at LHC: a serendipitous interplay of jet suppression and fragmentation*, *Phys. Rev. Lett.* **112** (2014) 042302 [arXiv:1307.4702] [INSPIRE].

[61] A. Beraudo, A. De Pace, M. Monteno, M. Nardi and F. Prino, *Heavy flavors in heavy-ion collisions: quenching, flow and correlations*, *Eur. Phys. J.* **C 75** (2015) 121 [arXiv:1410.6082] [INSPIRE].

[62] M. Nahrgang, J. Aichelin, P.B. Gossiaux and K. Werner, *Influence of hadronic bound states above T_c on heavy-quark observables in $Pb+Pb$ collisions at at the CERN Large Hadron Collider*, *Phys. Rev.* **C 89** (2014) 014905 [arXiv:1305.6544] [INSPIRE].

[63] T. Song, H. Berrehrah, D. Cabrera, W. Cassing and E. Bratkovskaya, *Charm production in $Pb+Pb$ collisions at energies available at the CERN Large Hadron Collider*, *Phys. Rev.* **C 93** (2016) 034906 [arXiv:1512.00891] [INSPIRE].

JHEP10(2018)174

[64] J. Xu, J. Liao and M. Gyulassy, *Bridging Soft-Hard Transport Properties of quark-gluon Plasmas with CUJET3.0*, *JHEP* **02** (2016) 169 [arXiv:1508.00552] [INSPIRE].

[65] Z.-B. Kang, F. Ringer and I. Vitev, *Effective field theory approach to open heavy flavor production in heavy-ion collisions*, *JHEP* **03** (2017) 146 [arXiv:1610.02043] [INSPIRE].

[66] ALICE collaboration, *D-meson azimuthal anisotropy in midcentral Pb-Pb collisions at* $\sqrt{s_{\rm NN}} = 5.02$ *TeV*, *Phys. Rev. Lett.* **120** (2018) 102301 [arXiv:1707.01005] [INSPIRE].

JHEP10(2018)174

The ALICE collaboration

S. Acharya[138], F.T.-. Acosta[22], D. Adamová[93], J. Adolfsson[80], M.M. Aggarwal[97], G. Aglieri Rinella[36], M. Agnello[33], N. Agrawal[48], Z. Ahammed[138], S.U. Ahn[76], S. Aiola[143], A. Akindinov[64], M. Al-Turany[103], S.N. Alam[138], D.S.D. Albuquerque[119], D. Aleksandrov[87], B. Alessandro[58], R. Alfaro Molina[72], Y. Ali[16], A. Alici[11,53,29], A. Alkin[3], J. Alme[24], T. Alt[69], L. Altenkamper[24], I. Altsybeev[137], C. Andrei[47], D. Andreou[36], H.A. Andrews[107], A. Andronic[103], M. Angeletti[36], V. Anguelov[101], C. Anson[17], T. Antičić[104], F. Antinori[56], P. Antonioli[53], R. Anwar[123], N. Apadula[79], L. Aphecetche[111], H. Appelshäuser[69], S. Arcelli[29], R. Arnaldi[58], O.W. Arnold[102,114], I.C. Arsene[23], M. Arslandok[101], B. Audurier[111], A. Augustinus[36], R. Averbeck[103], M.D. Azmi[18], A. Badalà[55], Y.W. Baek[60,41], S. Bagnasco[58], R. Bailhache[69], R. Bala[98], A. Baldisseri[134], M. Ball[43], R.C. Baral[85], A.M. Barbano[28], R. Barbera[30], F. Barile[52], L. Barioglio[28], G.G. Barnaföldi[142], L.S. Barnby[92], V. Barret[131], P. Bartalini[7], K. Barth[36], E. Bartsch[69], N. Bastid[131], S. Basu[140], G. Batigne[111], B. Batyunya[75], P.C. Batzing[23], J.L. Bazo Alba[108], I.G. Bearden[88], H. Beck[101], C. Bedda[63], N.K. Behera[60], I. Belikov[133], F. Bellini[29,36], H. Bello Martinez[2], R. Bellwied[123], L.G.E. Beltran[117], V. Belyaev[91], G. Bencedi[142], S. Beole[28], A. Bercuci[47], Y. Berdnikov[95], D. Berenyi[142], R.A. Bertens[127], D. Berzano[36,58], L. Betev[36], P.P. Bhaduri[138], A. Bhasin[98], I.R. Bhat[98], H. Bhatt[48], B. Bhattacharjee[42], J. Bhom[115], A. Bianchi[28], L. Bianchi[123], N. Bianchi[51], J. Bielčík[38], J. Bielčíková[93], A. Bilandzic[102,114], G. Biro[142], R. Biswas[4], S. Biswas[4], J.T. Blair[116], D. Blau[87], C. Blume[69], G. Boca[135], F. Bock[36], A. Bogdanov[91], L. Boldizsár[142], M. Bombara[39], G. Bonomi[136], M. Bonora[36], H. Borel[134], A. Borissov[141,20], M. Borri[125], E. Botta[28], C. Bourjau[88], L. Bratrud[69], P. Braun-Munzinger[103], M. Bregant[118], T.A. Broker[69], M. Broz[38], E.J. Brucken[44], E. Bruna[58], G.E. Bruno[36,35], D. Budnikov[105], H. Buesching[69], S. Bufalino[33], P. Buhler[110], P. Buncic[36], O. Busch[130], Z. Buthelezi[73], J.B. Butt[16], J.T. Buxton[19], J. Cabala[113], D. Caffarri[89], H. Caines[143], A. Caliva[103], E. Calvo Villar[108], R.S. Camacho[2], P. Camerini[27], A.A. Capon[110], F. Carena[36], W. Carena[36], F. Carnesecchi[29,11], J. Castillo Castellanos[134], A.J. Castro[127], E.A.R. Casula[54], C. Ceballos Sanchez[9], S. Chandra[138], B. Chang[124], W. Chang[7], S. Chapeland[36], M. Chartier[125], S. Chattopadhyay[138], S. Chattopadhyay[106], A. Chauvin[114,102], C. Cheshkov[132], B. Cheynis[132], V. Chibante Barroso[36], D.D. Chinellato[119], S. Cho[60], P. Chochula[36], T. Chowdhury[131], P. Christakoglou[89], C.H. Christensen[88], P. Christiansen[80], T. Chujo[130], S.U. Chung[20], C. Cicalo[54], L. Cifarelli[11,29], F. Cindolo[53], J. Cleymans[122], F. Colamaria[52], D. Colella[65,52,36], A. Collu[79], M. Colocci[29], M. Concas[58,i], G. Conesa Balbastre[78], Z. Conesa del Valle[61], J.G. Contreras[38], T.M. Cormier[94], Y. Corrales Morales[58], P. Cortese[34], M.R. Cosentino[120], F. Costa[36], S. Costanza[135], J. Crkovská[61], P. Crochet[131], E. Cuautle[70], L. Cunqueiro[94,141], T. Dahms[102,114], A. Dainese[56], M.C. Danisch[101], A. Danu[68], D. Das[106], I. Das[106], S. Das[4], A. Dash[85], S. Dash[48], S. De[49], A. De Caro[32], G. de Cataldo[52], C. de Conti[118], J. de Cuveland[40], A. De Falco[26], D. De Gruttola[11,32], N. De Marco[58], S. De Pasquale[32], R.D. De Souza[119], H.F. Degenhardt[118], A. Deisting[103,101], A. Deloff[84], S. Delsanto[28], C. Deplano[89], P. Dhankher[48], D. Di Bari[35], A. Di Mauro[36], B. Di Ruzza[56], R.A. Diaz[9], T. Dietel[122], P. Dillenseger[69], Y. Ding[7], R. Divià[36], Ø. Djuvsland[24], A. Dobrin[36], D. Domenicis Gimenez[118], B. Dönigus[69], O. Dordic[23], L.V.R. Doremalen[63], A.K. Dubey[138], A. Dubla[103], L. Ducroux[132], S. Dudi[97], A.K. Duggal[97], M. Dukhishyam[85], P. Dupieux[131], R.J. Ehlers[143], D. Elia[52], E. Endress[108], H. Engel[74], E. Epple[143], B. Erazmus[111], F. Erhardt[96], M.R. Ersdal[24], B. Espagnon[61], G. Eulisse[36], J. Eum[20], D. Evans[107], S. Evdokimov[90], L. Fabbietti[102,114], M. Faggin[31], J. Faivre[78], A. Fantoni[51], M. Fasel[94], L. Feldkamp[141], A. Feliciello[58], G. Feofilov[137], A. Fernández Téllez[2], A. Ferretti[28], A. Festanti[31,36], V.J.G. Feuillard[134,131], J. Figiel[115], M.A.S. Figueredo[118], S. Filchagin[105], D. Finogeev[62], F.M. Fionda[24], G. Fiorenza[52], M. Floris[36],

JHEP10(2018)174

S. Foertsch[73], P. Foka[103], S. Fokin[87], E. Fragiacomo[59], A. Francescon[36], A. Francisco[111], U. Frankenfeld[103], G.G. Fronze[28], U. Fuchs[36], C. Furget[78], A. Furs[62], M. Fusco Girard[32], J.J. Gaardhøje[88], M. Gagliardi[28], A.M. Gago[108], K. Gajdosova[88], M. Gallio[28], C.D. Galvan[117], P. Ganoti[83], C. Garabatos[103], E. Garcia-Solis[12], K. Garg[30], C. Gargiulo[36], P. Gasik[102,114], E.F. Gauger[116], M.B. Gay Ducati[71], M. Germain[111], J. Ghosh[106], P. Ghosh[138], S.K. Ghosh[4], P. Gianotti[51], P. Giubellino[58,103], P. Giubilato[31], P. Glässel[101], D.M. Goméz Coral[72], A. Gomez Ramirez[74], V. Gonzalez[103], P. González-Zamora[2], S. Gorbunov[40], L. Görlich[115], S. Gotovac[126], V. Grabski[72], L.K. Graczykowski[139], K.L. Graham[107], L. Greiner[79], A. Grelli[63], C. Grigoras[36], V. Grigoriev[91], A. Grigoryan[1], S. Grigoryan[75], J.M. Gronefeld[103], F. Grosa[33], J.F. Grosse-Oetringhaus[36], R. Grosso[103], R. Guernane[78], B. Guerzoni[29], M. Guittiere[111], K. Gulbrandsen[88], T. Gunji[129], A. Gupta[98], R. Gupta[98], I.B. Guzman[2], R. Haake[36], M.K. Habib[103], C. Hadjidakis[61], H. Hamagaki[81], G. Hamar[142], J.C. Hamon[133], M.R. Haque[63], J.W. Harris[143], A. Harton[12], H. Hassan[78], D. Hatzifotiadou[53,11], S. Hayashi[129], S.T. Heckel[69], E. Hellbär[69], H. Helstrup[37], A. Herghelegiu[47], E.G. Hernandez[2], G. Herrera Corral[10], F. Herrmann[141], K.F. Hetland[37], T.E. Hilden[44], H. Hillemanns[36], C. Hills[125], B. Hippolyte[133], B. Hohlweger[102], D. Horak[38], S. Hornung[103], R. Hosokawa[130,78], P. Hristov[36], C. Hughes[127], P. Huhn[69], T.J. Humanic[19], H. Hushnud[106], N. Hussain[42], T. Hussain[18], D. Hutter[40], D.S. Hwang[21], J.P. Iddon[125], S.A. Iga Buitron[70], R. Ilkaev[105], M. Inaba[130], M. Ippolitov[87], M.S. Islam[106], M. Ivanov[103], V. Ivanov[95], V. Izucheev[90], B. Jacak[79], N. Jacazio[29], P.M. Jacobs[79], M.B. Jadhav[48], S. Jadlovska[113], J. Jadlovsky[113], S. Jaelani[63], C. Jahnke[118,114], M.J. Jakubowska[139], M.A. Janik[139], C. Jena[85], M. Jercic[96], R.T. Jimenez Bustamante[103], M. Jin[123], P.G. Jones[107], A. Jusko[107], P. Kalinak[65], A. Kalweit[36], J.H. Kang[144], V. Kaplin[91], S. Kar[7], A. Karasu Uysal[77], O. Karavichev[62], T. Karavicheva[62], P. Karczmarczyk[36], E. Karpechev[62], U. Kebschull[74], R. Keidel[46], D.L.D. Keijdener[63], M. Keil[36], B. Ketzer[43], Z. Khabanova[89], S. Khan[18], S.A. Khan[138], A. Khanzadeev[95], Y. Kharlov[90], A. Khatun[18], A. Khuntia[49], M.M. Kielbowicz[115], B. Kileng[37], B. Kim[130], D. Kim[144], D.J. Kim[124], E.J. Kim[14], H. Kim[144], J.S. Kim[41], J. Kim[101], M. Kim[101,60], S. Kim[21], T. Kim[144], T. Kim[144], S. Kirsch[40], I. Kisel[40], S. Kiselev[64], A. Kisiel[139], J.L. Klay[6], C. Klein[69], J. Klein[36,58], C. Klein-Bösing[141], S. Klewin[101], A. Kluge[36], M.L. Knichel[101,36], A.G. Knospe[123], C. Kobdaj[112], M. Kofarago[142], M.K. Köhler[101], T. Kollegger[103], N. Kondratyeva[91], E. Kondratyuk[90], A. Konevskikh[62], M. Konyushikhin[140], O. Kovalenko[84], V. Kovalenko[137], M. Kowalski[115], I. Králik[65], A. Kravčáková[39], L. Kreis[103], M. Krivda[65,107], F. Krizek[93], M. Krüger[69], E. Kryshen[95], M. Krzewicki[40], A.M. Kubera[19], V. Kučera[60,93], C. Kuhn[133], P.G. Kuijer[89], J. Kumar[48], L. Kumar[97], S. Kumar[48], S. Kundu[85], P. Kurashvili[84], A. Kurepin[62], A.B. Kurepin[62], A. Kuryakin[105], S. Kushpil[93], M.J. Kweon[60], Y. Kwon[144], S.L. La Pointe[40], P. La Rocca[30], Y.S. Lai[79], I. Lakomov[36], R. Langoy[121], K. Lapidus[143], C. Lara[74], A. Lardeux[23], P. Larionov[51], A. Lattuca[28], E. Laudi[36], R. Lavicka[38], R. Lea[27], L. Leardini[101], S. Lee[144], F. Lehas[89], S. Lehner[110], J. Lehrbach[40], R.C. Lemmon[92], E. Leogrande[63], I. León Monzón[117], P. Lévai[142], X. Li[13], X.L. Li[7], J. Lien[121], R. Lietava[107], B. Lim[20], S. Lindal[23], V. Lindenstruth[40], S.W. Lindsay[125], C. Lippmann[103], M.A. Lisa[19], V. Litichevskyi[44], A. Liu[79], H.M. Ljunggren[80], W.J. Llope[140], D.F. Lodato[63], V. Loginov[91], C. Loizides[79,94], P. Loncar[126], X. Lopez[131], E. López Torres[9], A. Lowe[142], P. Luettig[69], J.R. Luhder[141], M. Lunardon[31], G. Luparello[59], M. Lupi[36], A. Maevskaya[62], M. Mager[36], S.M. Mahmood[23], A. Maire[133], R.D. Majka[143], M. Malaev[95], L. Malinina[75, ii], D. Mal'Kevich[64], P. Malzacher[103], A. Mamonov[105], V. Manko[87], F. Manso[131], V. Manzari[52], Y. Mao[7], M. Marchisone[132,128,73], J. Mareš[67], G.V. Margagliotti[27], A. Margotti[53], J. Margutti[63], A. Marín[103], C. Markert[116], M. Marquard[69], N.A. Martin[103], P. Martinengo[36], M.I. Martínez[2], G. Martínez García[111], M. Martinez Pedreira[36], S. Masciocchi[103], M. Masera[28], A. Masoni[54], L. Massacrier[61], E. Masson[111], A. Mastroserio[52], A.M. Mathis[102,114],

JHEP10(2018)174

P.F.T. Matuoka[118], A. Matyja[115,127], C. Mayer[115], M. Mazzilli[35], M.A. Mazzoni[57], F. Meddi[25], Y. Melikyan[91], A. Menchaca-Rocha[72], E. Meninno[32], J. Mercado Pérez[101], M. Meres[15], C.S. Meza[108], S. Mhlanga[122], Y. Miake[130], L. Micheletti[28], M.M. Mieskolainen[44], D.L. Mihaylov[102], K. Mikhaylov[64,75], A. Mischke[63], A.N. Mishra[70], D. Miśkowiec[103], J. Mitra[138], C.M. Mitu[68], N. Mohammadi[36,63], A.P. Mohanty[63], B. Mohanty[85], M. Mohisin Khan[18, iii], D.A. Moreira De Godoy[141], L.A.P. Moreno[2], S. Moretto[31], A. Morreale[111], A. Morsch[36], V. Muccifora[51], E. Mudnic[126], D. Mühlheim[141], S. Muhuri[138], M. Mukherjee[4], J.D. Mulligan[143], M.G. Munhoz[118], K. Münning[43], M.I.A. Munoz[79], R.H. Munzer[69], H. Murakami[129], S. Murray[73], L. Musa[36], J. Musinsky[65], C.J. Myers[123], J.W. Myrcha[139], B. Naik[48], R. Nair[84], B.K. Nandi[48], R. Nania[53,11], E. Nappi[52], A. Narayan[48], M.U. Naru[16], H. Natal da Luz[118], C. Nattrass[127], S.R. Navarro[2], K. Nayak[85], R. Nayak[48], T.K. Nayak[138], S. Nazarenko[105], R.A. Negrao De Oliveira[69,36], L. Nellen[70], S.V. Nesbo[37], G. Neskovic[40], F. Ng[123], M. Nicassio[103], J. Niedziela[139,36], B.S. Nielsen[88], S. Nikolaev[87], S. Nikulin[87], V. Nikulin[95], F. Noferini[11,53], P. Nomokonov[75], G. Nooren[63], J.C.C. Noris[2], J. Norman[78,125], A. Nyanin[87], J. Nystrand[24], H. Oh[144], A. Ohlson[101], J. Oleniacz[139], A.C. Oliveira Da Silva[118], M.H. Oliver[143], J. Onderwaater[103], C. Oppedisano[58], R. Orava[44], M. Oravec[113], A. Ortiz Velasquez[70], A. Oskarsson[80], J. Otwinowski[115], K. Oyama[81], Y. Pachmayer[101], V. Pacik[88], D. Pagano[136], G. Paić[70], P. Palni[7], J. Pan[140], A.K. Pandey[48], S. Panebianco[134], V. Papikyan[1], P. Pareek[49], J. Park[60], J.E. Parkkila[124], S. Parmar[97], A. Passfeld[141], S.P. Pathak[123], R.N. Patra[138], B. Paul[58], H. Pei[7], T. Peitzmann[63], X. Peng[7], L.G. Pereira[71], H. Pereira Da Costa[134], D. Peresunko[87], E. Perez Lezama[69], V. Peskov[69], Y. Pestov[5], V. Petráček[38], M. Petrovici[47], C. Petta[30], R.P. Pezzi[71], S. Piano[59], M. Pikna[15], P. Pillot[111], L.O.D.L. Pimentel[88], O. Pinazza[53,36], L. Pinsky[123], S. Pisano[51], D.B. Piyarathna[123], M. Płoskoń[79], M. Planinic[96], F. Pliquett[69], J. Pluta[139], S. Pochybova[142], P.L.M. Podesta-Lerma[117], M.G. Poghosyan[94], B. Polichtchouk[90], N. Poljak[96], W. Poonsawat[112], A. Pop[47], H. Poppenborg[141], S. Porteboeuf-Houssais[131], V. Pozdniakov[75], S.K. Prasad[4], R. Preghenella[53], F. Prino[58], C.A. Pruneau[140], I. Pshenichnov[62], M. Puccio[28], V. Punin[105], J. Putschke[140], S. Raha[4], S. Rajput[98], J. Rak[124], A. Rakotozafindrabe[134], L. Ramello[34], F. Rami[133], R. Raniwala[99], S. Raniwala[99], S.S. Räsänen[44], B.T. Rascanu[69], V. Ratza[43], I. Ravasenga[33], K.F. Read[127,94], K. Redlich[84, iv], A. Rehman[24], P. Reichelt[69], F. Reidt[36], X. Ren[7], R. Renfordt[69], A. Reshetin[62], J.-P. Revol[11], K. Reygers[101], V. Riabov[95], T. Richert[63,80], M. Richter[23], P. Riedler[36], W. Riegler[36], F. Riggi[30], C. Ristea[68], M. Rodríguez Cahuantzi[2], K. Røed[23], R. Rogalev[90], E. Rogochaya[75], D. Rohr[36], D. Röhrich[24], P.S. Rokita[139], F. Ronchetti[51], E.D. Rosas[70], K. Roslon[139], P. Rosnet[131], A. Rossi[31,56], A. Rotondi[135], F. Roukoutakis[83], C. Roy[133], P. Roy[106], O.V. Rueda[70], R. Rui[27], B. Rumyantsev[75], A. Rustamov[86], E. Ryabinkin[87], Y. Ryabov[95], A. Rybicki[115], S. Saarinen[44], S. Sadhu[138], S. Sadovsky[90], K. Šafařík[36], S.K. Saha[138], B. Sahoo[48], P. Sahoo[49], R. Sahoo[49], S. Sahoo[66], P.K. Sahu[66], J. Saini[138], S. Sakai[130], M.A. Saleh[140], S. Sambyal[98], V. Samsonov[95,91], A. Sandoval[72], A. Sarkar[73], D. Sarkar[138], N. Sarkar[138], P. Sarma[42], M.H.P. Sas[63], E. Scapparone[53], F. Scarlassara[31], B. Schaefer[94], H.S. Scheid[69], C. Schiaua[47], R. Schicker[101], C. Schmidt[103], H.R. Schmidt[100], M.O. Schmidt[101], M. Schmidt[100], N.V. Schmidt[94,69], J. Schukraft[36], Y. Schutz[36,133], K. Schwarz[103], K. Schweda[103], G. Scioli[29], E. Scomparin[58], M. Šefčík[39], J.E. Seger[17], Y. Sekiguchi[129], D. Sekihata[45], I. Selyuzhenkov[91,103], K. Senosi[73], S. Senyukov[133], E. Serradilla[72], P. Sett[48], A. Sevcenco[68], A. Shabanov[62], A. Shabetai[111], R. Shahoyan[36], W. Shaikh[106], A. Shangaraev[90], A. Sharma[97], A. Sharma[98], N. Sharma[97], A.I. Sheikh[138], K. Shigaki[45], M. Shimomura[82], S. Shirinkin[64], Q. Shou[7,109], K. Shtejer[28], Y. Sibiriak[87], S. Siddhanta[54], K.M. Sielewicz[36], T. Siemiarczuk[84], D. Silvermyr[80], G. Simatovic[89], G. Simonetti[102,36], R. Singaraju[138], R. Singh[85], V. Singhal[138], T. Sinha[106], B. Sitar[15], M. Sitta[34], T.B. Skaali[23], M. Slupecki[124], N. Smirnov[143], R.J.M. Snellings[63], T.W. Snellman[124], J. Song[20],

JHEP10(2018)174

F. Soramel[31], S. Sorensen[127], F. Sozzi[103], I. Sputowska[115], J. Stachel[101], I. Stan[68], P. Stankus[94], E. Stenlund[80], D. Stocco[111], M.M. Storetvedt[37], P. Strmen[15], A.A.P. Suaide[118], T. Sugitate[45], C. Suire[61], M. Suleymanov[16], M. Suljic[36,27], R. Sultanov[64], M. Šumbera[93], S. Sumowidagdo[50], K. Suzuki[110], S. Swain[66], A. Szabo[15], I. Szarka[15], U. Tabassam[16], J. Takahashi[119], G.J. Tambave[24], N. Tanaka[130], M. Tarhini[61,111], M. Tariq[18], M.G. Tarzila[47], A. Tauro[36], G. Tejeda Muñoz[2], A. Telesca[36], C. Terrevoli[31], B. Teyssier[132], D. Thakur[49], S. Thakur[138], D. Thomas[116], F. Thoresen[88], R. Tieulent[132], A. Tikhonov[62], A.R. Timmins[123], A. Toia[69], N. Topilskaya[62], M. Toppi[51], S.R. Torres[117], S. Tripathy[49], S. Trogolo[28], G. Trombetta[35], L. Tropp[39], V. Trubnikov[3], W.H. Trzaska[124], T.P. Trzcinski[139], B.A. Trzeciak[63], T. Tsuji[129], A. Tumkin[105], R. Turrisi[56], T.S. Tveter[23], K. Ullaland[24], E.N. Umaka[123], A. Uras[132], G.L. Usai[26], A. Utrobicic[96], M. Vala[113], J.W. Van Hoorne[36], M. van Leeuwen[63], P. Vande Vyvre[36], D. Varga[142], A. Vargas[2], M. Vargyas[124], R. Varma[48], M. Vasileiou[83], A. Vasiliev[87], A. Vauthier[78], O. Vázquez Doce[102,114], V. Vechernin[137], A.M. Veen[63], A. Velure[24], E. Vercellin[28], S. Vergara Limón[2], L. Vermunt[63], R. Vernet[8], R. Vértesi[142], L. Vickovic[126], J. Viinikainen[124], Z. Vilakazi[128], O. Villalobos Baillie[107], A. Villatoro Tello[2], A. Vinogradov[87], T. Virgili[32], V. Vislavicius[80], A. Vodopyanov[75], M.A. Völkl[100], K. Voloshin[64], S.A. Voloshin[140], G. Volpe[35], B. von Haller[36], I. Vorobyev[114,102], D. Voscek[113], D. Vranic[103,36], J. Vrláková[39], B. Wagner[24], H. Wang[63], M. Wang[7], Y. Watanabe[130,129], M. Weber[110], S.G. Weber[103], A. Wegrzynek[36], D.F. Weiser[101], S.C. Wenzel[36], J.P. Wessels[141], U. Westerhoff[141], A.M. Whitehead[122], J. Wiechula[69], J. Wikne[23], G. Wilk[84], J. Wilkinson[53], G.A. Willems[141,36], M.C.S. Williams[53], E. Willsher[107], B. Windelband[101], W.E. Witt[127], R. Xu[7], S. Yalcin[77], K. Yamakawa[45], S. Yano[45], Z. Yin[7], H. Yokoyama[130,78], I.-K. Yoo[20], J.H. Yoon[60], V. Yurchenko[3], V. Zaccolo[58], A. Zaman[16], C. Zampolli[36], H.J.C. Zanoli[118], N. Zardoshti[107], A. Zarochentsev[137], P. Závada[67], N. Zaviyalov[105], H. Zbroszczyk[139], M. Zhalov[95], X. Zhang[7], Y. Zhang[7], Z. Zhang[131,7], C. Zhao[23], V. Zherebchevskii[137], N. Zhigareva[64], D. Zhou[7], Y. Zhou[88], Z. Zhou[24], H. Zhu[7], J. Zhu[7], Y. Zhu[7], A. Zichichi[29,11], M.B. Zimmermann[36], G. Zinovjev[3], J. Zmeskal[110], S. Zou[7]

[i] *Dipartimento DET del Politecnico di Torino, Turin, Italy*
[ii] *M.V. Lomonosov Moscow State University, D.V. Skobeltsyn Institute of Nuclear, Physics, Moscow, Russia*
[iii] *Department of Applied Physics, Aligarh Muslim University, Aligarh, India*
[iv] *Institute of Theoretical Physics, University of Wroclaw, Poland*

[1] *A.I. Alikhanyan National Science Laboratory (Yerevan Physics Institute) Foundation, Yerevan, Armenia*
[2] *Benemérita Universidad Autónoma de Puebla, Puebla, Mexico*
[3] *Bogolyubov Institute for Theoretical Physics, National Academy of Sciences of Ukraine, Kiev, Ukraine*
[4] *Bose Institute, Department of Physics and Centre for Astroparticle Physics and Space Science (CAPSS), Kolkata, India*
[5] *Budker Institute for Nuclear Physics, Novosibirsk, Russia*
[6] *California Polytechnic State University, San Luis Obispo, California, United States*
[7] *Central China Normal University, Wuhan, China*
[8] *Centre de Calcul de l'IN2P3, Villeurbanne, Lyon, France*
[9] *Centro de Aplicaciones Tecnológicas y Desarrollo Nuclear (CEADEN), Havana, Cuba*
[10] *Centro de Investigación y de Estudios Avanzados (CINVESTAV), Mexico City and Mérida, Mexico*
[11] *Centro Fermi - Museo Storico della Fisica e Centro Studi e Ricerche 'Enrico Fermi', Rome, Italy*
[12] *Chicago State University, Chicago, Illinois, United States*
[13] *China Institute of Atomic Energy, Beijing, China*
[14] *Chonbuk National University, Jeonju, Republic of Korea*

JHEP10(2018)174

[15] *Comenius University Bratislava, Faculty of Mathematics, Physics and Informatics, Bratislava, Slovakia*
[16] *COMSATS Institute of Information Technology (CIIT), Islamabad, Pakistan*
[17] *Creighton University, Omaha, Nebraska, United States*
[18] *Department of Physics, Aligarh Muslim University, Aligarh, India*
[19] *Department of Physics, Ohio State University, Columbus, Ohio, United States*
[20] *Department of Physics, Pusan National University, Pusan, Republic of Korea*
[21] *Department of Physics, Sejong University, Seoul, Republic of Korea*
[22] *Department of Physics, University of California, Berkeley, California, United States*
[23] *Department of Physics, University of Oslo, Oslo, Norway*
[24] *Department of Physics and Technology, University of Bergen, Bergen, Norway*
[25] *Dipartimento di Fisica dell'Università 'La Sapienza' and Sezione INFN, Rome, Italy*
[26] *Dipartimento di Fisica dell'Università and Sezione INFN, Cagliari, Italy*
[27] *Dipartimento di Fisica dell'Università and Sezione INFN, Trieste, Italy*
[28] *Dipartimento di Fisica dell'Università and Sezione INFN, Turin, Italy*
[29] *Dipartimento di Fisica e Astronomia dell'Università and Sezione INFN, Bologna, Italy*
[30] *Dipartimento di Fisica e Astronomia dell'Università and Sezione INFN, Catania, Italy*
[31] *Dipartimento di Fisica e Astronomia dell'Università and Sezione INFN, Padova, Italy*
[32] *Dipartimento di Fisica 'E.R. Caianiello' dell'Università and Gruppo Collegato INFN, Salerno, Italy*
[33] *Dipartimento DISAT del Politecnico and Sezione INFN, Turin, Italy*
[34] *Dipartimento di Scienze e Innovazione Tecnologica dell'Università del Piemonte Orientale and INFN Sezione di Torino, Alessandria, Italy*
[35] *Dipartimento Interateneo di Fisica 'M. Merlin' and Sezione INFN, Bari, Italy*
[36] *European Organization for Nuclear Research (CERN), Geneva, Switzerland*
[37] *Faculty of Engineering and Science, Western Norway University of Applied Sciences, Bergen, Norway*
[38] *Faculty of Nuclear Sciences and Physical Engineering, Czech Technical University in Prague, Prague, Czech Republic*
[39] *Faculty of Science, P.J. Šafárik University, Košice, Slovakia*
[40] *Frankfurt Institute for Advanced Studies, Johann Wolfgang Goethe-Universität Frankfurt, Frankfurt, Germany*
[41] *Gangneung-Wonju National University, Gangneung, Republic of Korea*
[42] *Gauhati University, Department of Physics, Guwahati, India*
[43] *Helmholtz-Institut für Strahlen- und Kernphysik, Rheinische Friedrich-Wilhelms-Universität Bonn, Bonn, Germany*
[44] *Helsinki Institute of Physics (HIP), Helsinki, Finland*
[45] *Hiroshima University, Hiroshima, Japan*
[46] *Hochschule Worms, Zentrum für Technologietransfer und Telekommunikation (ZTT), Worms, Germany*
[47] *Horia Hulubei National Institute of Physics and Nuclear Engineering, Bucharest, Romania*
[48] *Indian Institute of Technology Bombay (IIT), Mumbai, India*
[49] *Indian Institute of Technology Indore, Indore, India*
[50] *Indonesian Institute of Sciences, Jakarta, Indonesia*
[51] *INFN, Laboratori Nazionali di Frascati, Frascati, Italy*
[52] *INFN, Sezione di Bari, Bari, Italy*
[53] *INFN, Sezione di Bologna, Bologna, Italy*
[54] *INFN, Sezione di Cagliari, Cagliari, Italy*
[55] *INFN, Sezione di Catania, Catania, Italy*
[56] *INFN, Sezione di Padova, Padova, Italy*
[57] *INFN, Sezione di Roma, Rome, Italy*
[58] *INFN, Sezione di Torino, Turin, Italy*
[59] *INFN, Sezione di Trieste, Trieste, Italy*

JHEP10(2018)174

[60] Inha University, Incheon, Republic of Korea
[61] Institut de Physique Nucléaire d'Orsay (IPNO),
Institut National de Physique Nucléaire et de Physique des Particules (IN2P3/CNRS),
Université de Paris-Sud, Université Paris-Saclay, Orsay, France
[62] Institute for Nuclear Research, Academy of Sciences, Moscow, Russia
[63] Institute for Subatomic Physics, Utrecht University/Nikhef, Utrecht, Netherlands
[64] Institute for Theoretical and Experimental Physics, Moscow, Russia
[65] Institute of Experimental Physics, Slovak Academy of Sciences, Košice, Slovakia
[66] Institute of Physics, Bhubaneswar, India
[67] Institute of Physics of the Czech Academy of Sciences, Prague, Czech Republic
[68] Institute of Space Science (ISS), Bucharest, Romania
[69] Institut für Kernphysik, Johann Wolfgang Goethe-Universität Frankfurt, Frankfurt, Germany
[70] Instituto de Ciencias Nucleares, Universidad Nacional Autónoma de México, Mexico City, Mexico
[71] Instituto de Física, Universidade Federal do Rio Grande do Sul (UFRGS), Porto Alegre, Brazil
[72] Instituto de Física, Universidad Nacional Autónoma de México, Mexico City, Mexico
[73] iThemba LABS, National Research Foundation, Somerset West, South Africa
[74] Johann-Wolfgang-Goethe Universität Frankfurt Institut für Informatik,
Fachbereich Informatik und Mathematik, Frankfurt, Germany
[75] Joint Institute for Nuclear Research (JINR), Dubna, Russia
[76] Korea Institute of Science and Technology Information, Daejeon, Republic of Korea
[77] KTO Karatay University, Konya, Turkey
[78] Laboratoire de Physique Subatomique et de Cosmologie, Université Grenoble-Alpes, CNRS-IN2P3,
Grenoble, France
[79] Lawrence Berkeley National Laboratory, Berkeley, California, United States
[80] Lund University Department of Physics, Division of Particle Physics, Lund, Sweden
[81] Nagasaki Institute of Applied Science, Nagasaki, Japan
[82] Nara Women's University (NWU), Nara, Japan
[83] National and Kapodistrian University of Athens, School of Science, Department of Physics,
Athens, Greece
[84] National Centre for Nuclear Research, Warsaw, Poland
[85] National Institute of Science Education and Research, HBNI, Jatni, India
[86] National Nuclear Research Center, Baku, Azerbaijan
[87] National Research Centre Kurchatov Institute, Moscow, Russia
[88] Niels Bohr Institute, University of Copenhagen, Copenhagen, Denmark
[89] Nikhef, National institute for subatomic physics, Amsterdam, Netherlands
[90] NRC Kurchatov Institute, IHEP, Protvino, Russia
[91] NRNU Moscow Engineering Physics Institute, Moscow, Russia
[92] Nuclear Physics Group, STFC Daresbury Laboratory, Daresbury, United Kingdom
[93] Nuclear Physics Institute of the Czech Academy of Sciences, Řež u Prahy, Czech Republic
[94] Oak Ridge National Laboratory, Oak Ridge, Tennessee, United States
[95] Petersburg Nuclear Physics Institute, Gatchina, Russia
[96] Physics department, Faculty of science, University of Zagreb, Zagreb, Croatia
[97] Physics Department, Panjab University, Chandigarh, India
[98] Physics Department, University of Jammu, Jammu, India
[99] Physics Department, University of Rajasthan, Jaipur, India
[100] Physikalisches Institut, Eberhard-Karls-Universität Tübingen, Tübingen, Germany
[101] Physikalisches Institut, Ruprecht-Karls-Universität Heidelberg, Heidelberg, Germany
[102] Physik Department, Technische Universität München, Munich, Germany
[103] Research Division and ExtreMe Matter Institute EMMI,
GSI Helmholtzzentrum für Schwerionenforschung GmbH, Darmstadt, Germany
[104] Rudjer Bošković Institute, Zagreb, Croatia
[105] Russian Federal Nuclear Center (VNIIEF), Sarov, Russia

JHEP10(2018)174

[106] *Saha Institute of Nuclear Physics, Kolkata, India*
[107] *School of Physics and Astronomy, University of Birmingham, Birmingham, United Kingdom*
[108] *Sección Física, Departamento de Ciencias, Pontificia Universidad Católica del Perú, Lima, Peru*
[109] *Shanghai Institute of Applied Physics, Shanghai, China*
[110] *Stefan Meyer Institut für Subatomare Physik (SMI), Vienna, Austria*
[111] *SUBATECH, IMT Atlantique, Université de Nantes, CNRS-IN2P3, Nantes, France*
[112] *Suranaree University of Technology, Nakhon Ratchasima, Thailand*
[113] *Technical University of Košice, Košice, Slovakia*
[114] *Technische Universität München, Excellence Cluster 'Universe', Munich, Germany*
[115] *The Henryk Niewodniczanski Institute of Nuclear Physics, Polish Academy of Sciences, Cracow, Poland*
[116] *The University of Texas at Austin, Austin, Texas, United States*
[117] *Universidad Autónoma de Sinaloa, Culiacán, Mexico*
[118] *Universidade de São Paulo (USP), São Paulo, Brazil*
[119] *Universidade Estadual de Campinas (UNICAMP), Campinas, Brazil*
[120] *Universidade Federal do ABC, Santo Andre, Brazil*
[121] *University College of Southeast Norway, Tonsberg, Norway*
[122] *University of Cape Town, Cape Town, South Africa*
[123] *University of Houston, Houston, Texas, United States*
[124] *University of Jyväskylä, Jyväskylä, Finland*
[125] *University of Liverpool, Department of Physics Oliver Lodge Laboratory, Liverpool, United Kingdom*
[126] *University of Split, Faculty of Electrical Engineering, Mechanical Engineering and Naval Architecture, Split, Croatia*
[127] *University of Tennessee, Knoxville, Tennessee, United States*
[128] *University of the Witwatersrand, Johannesburg, South Africa*
[129] *University of Tokyo, Tokyo, Japan*
[130] *University of Tsukuba, Tsukuba, Japan*
[131] *Université Clermont Auvergne, CNRS/IN2P3, LPC, Clermont-Ferrand, France*
[132] *Université de Lyon, Université Lyon 1, CNRS/IN2P3, IPN-Lyon, Villeurbanne, Lyon, France*
[133] *Université de Strasbourg, CNRS, IPHC UMR 7178, F-67000 Strasbourg, France, Strasbourg, France*
[134] *Université Paris-Saclay Centre dÉtudes de Saclay (CEA), IRFU, Department de Physique Nucléaire (DPhN), Saclay, France*
[135] *Università degli Studi di Pavia, Pavia, Italy*
[136] *Università di Brescia, Brescia, Italy*
[137] *V. Fock Institute for Physics, St. Petersburg State University, St. Petersburg, Russia*
[138] *Variable Energy Cyclotron Centre, Kolkata, India*
[139] *Warsaw University of Technology, Warsaw, Poland*
[140] *Wayne State University, Detroit, Michigan, United States*
[141] *Westfälische Wilhelms-Universität Münster, Institut für Kernphysik, Münster, Germany*
[142] *Wigner Research Centre for Physics, Hungarian Academy of Sciences, Budapest, Hungary*
[143] *Yale University, New Haven, Connecticut, United States*
[144] *Yonsei University, Seoul, Republic of Korea*

JHEP10(2018)174